

Review

# Upgrading Lignocellulosic Biomasses: Hydrogenolysis of Platform Derived Molecules Promoted by Heterogeneous Pd-Fe Catalysts

Claudia Espro <sup>1</sup>, Bianca Gumina <sup>1</sup>, Emilia Paone <sup>2</sup> and Francesco Mauriello <sup>2,\*</sup>

<sup>1</sup> Dipartimento di Ingegneria, Università di Messina, Contrada di Dio Vill. S. Agata, I-98166 Messina, Italy; espro@unime.it (C.E.); bianca.gumina@unime.it (B.G.)

<sup>2</sup> Dipartimento DICEAM, Università Mediterranea di Reggio Calabria, Loc. Feo di Vito, I-89122 Reggio Calabria, Italy; emilia.paone@unirc.it

\* Correspondence: francesco.mauriello@unirc.it; Tel.: +39-0965-1692278

Academic Editor: Yu-Chuan Lin

Received: 30 December 2016; Accepted: 1 March 2017; Published: 7 March 2017

**Abstract:** This review provides an overview of heterogeneous bimetallic Pd-Fe catalysts in the C–C and C–O cleavage of platform molecules such as C2–C6 polyols, furfural, phenol derivatives and aromatic ethers that are all easily obtainable from renewable cellulose, hemicellulose and lignin (the major components of lignocellulosic biomasses). The interaction between palladium and iron affords bimetallic Pd-Fe sites (ensemble or alloy) that were found to be very active in several sustainable reactions including hydrogenolysis, catalytic transfer hydrogenolysis (CTH) and aqueous phase reforming (APR) that will be highlighted. This contribution concentrates also on the different synthetic strategies (incipient wetness impregnation, deposition-precipitation, co-precipitation) adopted for the preparation of heterogeneous Pd-Fe systems as well as on the main characterization techniques used (XRD, TEM, H<sub>2</sub>-TPR, XPS and EXAFS) in order to elucidate the key factors that influence the unique catalytic performances observed.

**Keywords:** heterogeneous catalysis; palladium; iron; iron oxides; bimetallic catalysts; cellulose; polyols; hemicellulose; furfural; lignin; phenol derivatives; aromatic ethers; hydrogenolysis; hydrodeoxygenation (HDO); catalytic transfer hydrogenolysis (CTH); aqueous phase reforming (APR)

## 1. Introduction

Modern chemical industry is facing the big challenge of overcoming its historical dependence on fossil resources by reconciling the economic recovery with the protection of environment and the reduction of greenhouse gas emissions. At the 21st United Nations Climate Change Conference (COP21), 195 nations agreed on a global action plan aimed to limit the global warming below 2 °C above pre-industrial levels. The “Paris Agreement” comes into force on the 4th November 2016 and is expected to be a new course in the global climate effort [1].

To achieve this ambitious goal, several countries are releasing new green economy strategies. USA have launched the “National Bioeconomy Blueprint Program” addressing five strategic objectives able to generate economic growth and to meet societal needs [2]. Accordingly, the EU has set a “Bioeconomy Strategy and Action Plan” [3–5] identifying, under the Framework Programme for Research and Innovation in Europe—Horizon 2020, seven priority challenges in research and innovation that can have a tangible effect on everyday life [6]. Asian countries, also due to their high growth rate of population, will be decisive for the development of sustainable biotechnologies, bio-industries and bio-refineries [7–9]. With the world population approaching about 9.6 billion by 2050 and limited natural reserves, the use of renewable resources is therefore essential for the sustainable supply of

bio-based building blocks and materials. Sorbitol, xylitol, glycerol and succinic acid are already produced from bio-based feedstock while other important intermediates including methanol, ethanol, 2-propanol, 2,5-furandicarboxylic acid and 3-hydroxypropanoic acid are expected to be made from renewable resources in the next few years [10]. According to latest forecast data, the global market of bio-chemicals is projected to reach about 100 billions of Euros in 2020, growing at a rate of about 13% over the period 2016–2022 [11,12].

To replace fossil-derived fuels and chemicals, the resources must be renewable, of sufficient abundance and not in competition with agricultural land and food production. Lignocellulosic biomasses are abundant and inedible resources that can be easily obtainable also from agricultural residues and waste. A variety of chemical routes and industrial processes have been explored to valorize lignocellulosic biomasses [13–23]. Since lignocellulose has a complex “chemical-architecture” [24], one strategy is the first deconstruction into cellulose, hemicellulose and lignin (Figure 1).

A wide variety of platform chemicals can be obtained from cellulose, hemicellulose and lignin. A non-exhaustive representation of the most important lignocellulosic-derived molecules for chemical industry are reported in Figure 2.

Cellulose, the largest single component of lignocellulosic biomasses, is a polymer of  $\beta$ -1,4-linked glucosidic units with an average molecular weight of around 100,000 that cannot be digested by humans [24]. Therefore, its utilization for chemicals production has not a negative impact on the food supply. For this reason, its conversion into added-value chemicals and/or fuel components is one of the core technologies in the modern bio-refinery [25–28]. The first step for cellulose valorization is based on its depolymerisation into oligomers and glucose followed by catalytic reactions (hydrogenation, oxidations, esterification, etc.) for the manufacture of a pool of chemicals such as C6–C2 polyols, levulinic acid, hydroxymethylfurfural (HMF), among others ([25–29] and “references within”). Polyols, owing to their peculiar chemical properties, could represent an important resource for production of several building-block chemicals. Sorbitol (C6 polyol), xylitol (C5 polyol) and glycerol (C3 polyol) have been included, by the USA Department of Energy, in the list of 12 potential biomass-derived platform chemicals [30]. Moreover, among the family of biomass derived polyols, glycerol (C3 polyol) has become a primary building block being the main by-product in the biodiesel production [31–38].

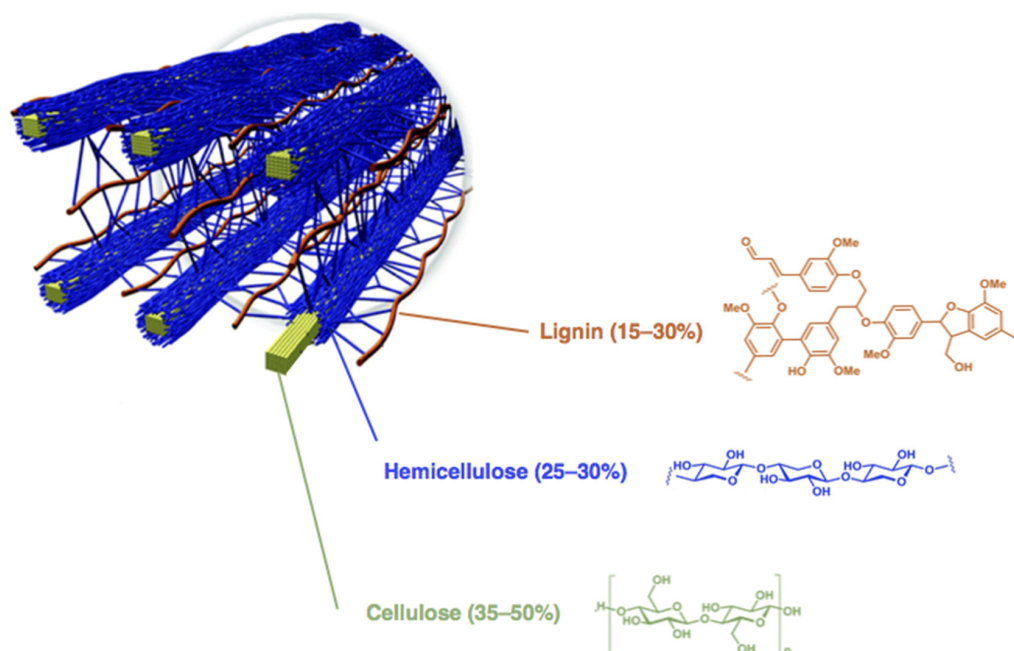


**Figure 1.** Arrangement of cellulose, hemicellulose and lignin in lignocellulosic biomasses. Adapted from <http://genomics.energy.gov> (accessed on 30 December 2016).

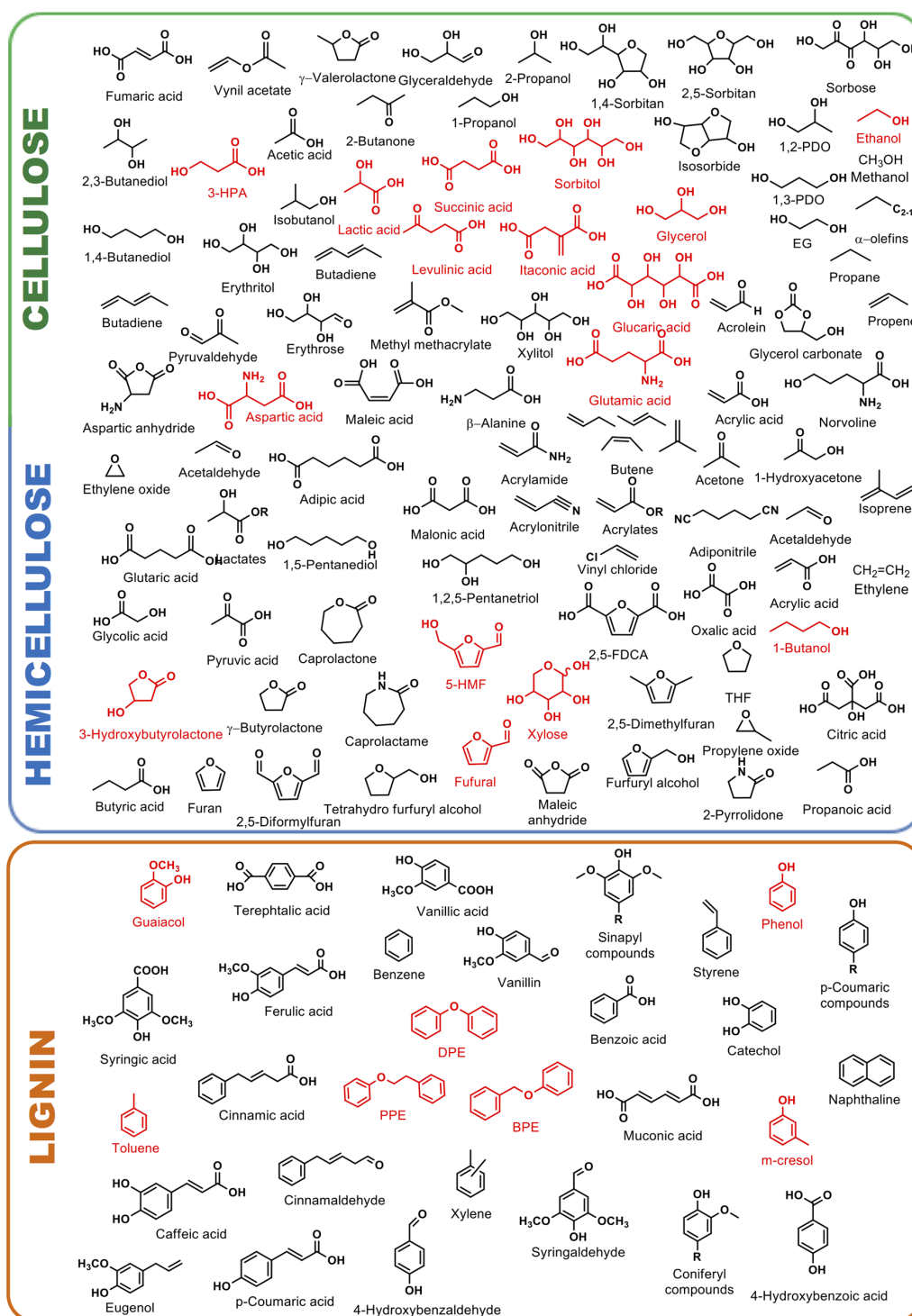


**Figure 2.** Building block chemicals that can be easily obtainable from catalytic upgrading of cellulose, hemicellulose and lignin (platform molecules are in red color).

Hemicellulose, unlike cellulose, has a heterogeneous chemical structure of pentoses, hexoses and sugar acids. Hardwood hemicelluloses is chiefly composed by xylans whereas softwood hemicellulose mainly consists of glucomannans [39,40]. Hemicellulose can be easily hydrolyzed into its sugar constituents by chemical or enzymatic processes [41–43]. The chemical hydrolysis of hemicelluloses into xylose and arabinose is generally afforded in high yields and low costs. Xylose, in particular, is largely used in modern biorefineries to produce furfural (2-furaldehyde) through

several homogeneous and heterogeneous catalytic processes [44]. Furfural, with a world production of about 200,000 tonnes per year, is the key precursor to important building blocks such as furfuryl alcohol, 2-methylfuran, 2-methyltetrahydrofuran and levulinic acid [45–47].

Lignin is unique among other biomass components, being characterized by an aromatic sub-structure with a large amount of etheric C–O bonds [24]. The native constituents of lignin are therefore of particular interest for a lignocellulosic biorefinery aimed to the sustainable production of green aromatic compounds. At present, industrial processes are limited to vanillin and “kraft lignin” (about 60 kt/year) manufacture but, the research on the sustainable production of chemicals from lignin has developed rapidly in the last years [48–52]. To this regard, one of the major challenges is the low cost-effective catalytic depolymerization of lignin preserving its aromatic nature [53–65].

One concern about the use of lignocellulosic biomasses in bio-refinery is that, if compared with fossil-derived feedstocks, they are characterized by a higher O/C ratio. Among several chemistries and technologies, hydrogenolysis processes have gained a lot of attention since it allows the breaking of carbon-carbon and/or carbon-oxygen bonds in the presence of a hydrogen source [66–68]. One of the main drawbacks in hydrogenolysis, also known as “hydrodeoxygenation” if referred to C–O bond breaking, is concerning the hydrogen management due to the poor solubility of molecular H<sub>2</sub> that leads to a considerable safety hazard. Moreover, hydrogen supply and related purchase, transport and storage costs need to be considered.

Alternatively to classic hydrogenolysis/hydrodeoxygenation processes, which generally require high pressure of molecular hydrogen, catalytic transfer hydrogenolysis (CTH) reactions by means of simple alcohols (2-propanol, methanol and ethanol) and other H-donor molecules (hydrazine, tetralin, formic acid, cyclohexene, etc.) have been generally proposed as an efficient alternative to the direct use of H<sub>2</sub> in the course of the last decade [69–72]. Since their debut in 1903 when Knoevenagel presented the disproportionation of dimethyl-1,4-dihydroterephthalate promoted by palladium black catalysts [73], CTH reactions are getting increasing attention improving the sustainability and economics of hydrogenation reactions in modern green chemistry since: (i) they do not require hazardous pressurized molecular hydrogen; (ii) the hydrogen donors are generally readily available, inexpensive, obtainable from renewable resources and easy to handle and (iii) they generally produce valuable by-products (i.e., oxidized alcohol products). Moreover, CTH has been successfully adopted in reducing oxygen content in biomass-derived feedstocks [72].

Another efficient route to obtain the hydrogen necessary for the cleavage of C–C and C–O bonds is directly from biomass-derived molecules by the aqueous phase reforming (APR) process [74–87]. The APR process presents many advantages than conventional steam reforming reactions because it occurs, under mild conditions, in liquid phase and in a single reactor. The APR process converts starting substrates into hydrogen through the breaking of C–C, C–H and O–H bonds and the simultaneous water-gas shift (WGS) reaction. In order to maximize the hydrogen production, a good APR catalyst needs to show significant activity in the C–C bond breaking and in the WGS reaction, but poor activity towards the C–O bond cleavage and methanation reaction.

Transition metals have been successfully used in the catalytic valorization of biomass-derived molecules. Traditionally, platinum-group metals (PGMm) are all excellent hydrogenation catalysts widely used in industry and refineries [88–91]. Palladium has a lower cost and more abundant reserves than platinum (that is still the most widely used element in catalysis) [92,93]. Homogeneous and heterogeneous palladium-based catalysts have found a potential application in several industrial reactions including hydrogenation, dehydrogenation, hydrogenolysis, reforming, oxidation, coupling reactions, carbonylation/decarbonylation and hydrodesulphurization [94–106]. With respect to other PGM elements, palladium is characterized by a fundamental electronic configuration unique among transition metals (4d<sup>10</sup>, 5s<sup>0</sup>) [107] that can be strongly influenced by the coordination environment [108]. The modification of catalytic properties of palladium by adding a second metal can be related, from a general point of view, in terms of (i) “ligand” effects (related to shifting of the d-band density); (ii) “ensemble” effect (a dilution of palladium surface by a relatively unreactive second co-metal);

(iii) “stabilizing” effect (improving the active sites stability) [109–114]. Hence, heterogeneous catalysts based on palladium bimetallic systems have gained increasing attention for their enhanced activity and durability in different reactions [115–189].

In this review, we focus our attention on heterogeneous bimetallic Pd-Fe catalysts that have been proved to show excellent performance in promoting the cleavage of C–O and C–C bond in platform derived molecules of cellulose, hemicellulose and lignin. Specifically, results obtained in important “green and sustainable” reactions will be presented including: aqueous-phase reforming [128–130], hydrogenolysis [131–136] and CTH [137,138] of C6–C2 polyols, hydrogenolysis and transfer hydrogenolysis of furfural [139,140], hydrodeoxygenation of phenol derivatives [141,142], HDO and CTH of aromatic ethers [143–145]. All these reactions will be discussed in details with the aim to show the unicity of heterogeneous Pd-Fe catalysts that are suitable for a wide reductive valorization processes of all constituent components of lignocellulosic biomasses having the potential to be successfully used in modern biorefineries to produce simple bulk compounds. The main peculiarity of these bimetallic catalysts is the formation of bimetallic Pd-Fe ensembles or alloys that allows modification of the electronic density of palladium thus promoting unexpected catalytic reactions under mild conditions. In addition, a close attention to different synthetic methods adopted for the preparation of heterogeneous Pd-Fe catalysts (Incipient Wetness Impregnation, Deposition-Precipitation and Co-precipitation) as well as to main characterization techniques used (X-ray Diffraction, Transmission Electron Microscopy, Hydrogen Temperature-Programmed Reduction, X-ray Photoelectron Spectroscopy, Extended X-ray Absorption Fine Structure) will be paid.

## 2. Synthesis and Characterization of Pd/Fe Catalysts

### 2.1. Preparation Methods

Preparation methods for the development of efficient bimetallic Pd-Fe catalysts were focused, in addition to the fundamental properties (activity, selectivity and stability) and practical applications (reuse, reproducibility and easy separation from the reaction mixture), on the optimization of metal-metal or metal/support interactions [116–125,190].

#### 2.1.1. Incipient Wetness Impregnation—IWi

In the “incipient wetness impregnation” (IWi) [191,192] preparation technique, the support is in contact with a definite volume of the precursor solution. This method was, so far, used for the synthesis of Pd/Fe<sub>3</sub>O<sub>4</sub> and Pd/Fe<sub>2</sub>O<sub>3</sub> catalysts [135,138,142,193]. In a typical preparation procedure, palladium (II) acetylacetonate is dissolved in acetone and then added to commercially available Fe<sub>3</sub>O<sub>4</sub> or Fe<sub>2</sub>O<sub>3</sub> supports [135,138,192]. After impregnation, samples are dried and reduced under a flow of molecular hydrogen. A similar procedure involves the filling of pores in the support, with a water solution of a suitable compound (e.g., a nitrate) that, when decomposed by heating, affords either the active phase itself or a compound that is easily converted into the active phase. This method was successfully utilized to obtain other Pd/Fe<sub>2</sub>O<sub>3</sub> catalysts with different Pd loading (0.1–5 wt %) [142]. In a typical synthesis process, the calcined Fe<sub>2</sub>O<sub>3</sub> powder (previously prepared by precipitation from the nitrate precursor with ammonium carbonate at room temperature and at pH 8.0) is impregnated into a Pd(NH<sub>3</sub>)<sub>4</sub>(NO<sub>3</sub>)<sub>2</sub> aqueous solution, followed by a drying process and subsequent calcination and reduction.

Other incipient wetness co-impregnation methods for preparing supported Pd-Fe bimetallic catalysts have been reported. An interesting approach, based on the use of a single step surfactant-templating procedure was used to prepare Pd-Fe/OMC supported catalysts [143,144]. The co-impregnation is fast and simple, but it is generally characterized by a poor interaction between the two precursors during the impregnation stage. The formation of bimetallic species generally takes place on the surface support throughout the reduction steps, with a consequent inhomogeneous distribution of the NPs on the catalyst surface, if the procedure is improperly carried out. To overcome

the limitations of the co-impregnation, it is advantageous to use the sequential impregnation, which consists of two stages. In the first step, Pd is supported by IWi and, in a subsequent stage, a Fe metal salt (generally nitrate) is added, also by IWi, to prepare the bimetallic catalyst. The sequential impregnation technique was used by Huber et al. [78,130], to prepare Pd-Fe bimetallic catalysts supported on  $\text{Al}_2\text{O}_3$ . By the same procedure a Pd-Fe/Zr-P bimetallic catalyst has been successfully obtained [140].

### 2.1.2. Deposition-Precipitation—DP

In the deposition-precipitation method (DP), the support material is deposited in an excess of the precursor solution in presence of a precipitation agent. The metal nanoparticles (NPs) nucleate and grow on the support surface. By this technique, a series of Pd nanoparticles on various iron oxides with different shape have been prepared [134].

### 2.1.3. Co-Precipitation—CP

The simultaneous precipitation of more than one precursor in a solution containing a precipitation agent (e.g., hydroxides, oxalates, formates, carbonates) is called co-precipitation [194,195]. After formation of the co-precipitate, hydrothermal treatments (which transform amorphous precipitates into crystalline materials with improved thermal stability and surface acidity) may be carried out. In catalysts with two or more metallic species, the final composition of the precipitate is governed by the differences in solubility between the components and the chemistry taking place during the precipitation process. Subsequently, to obtain crystalline stoichiometric precipitates with an intimate inter-dispersion of the two metals, several parameters (e.g., pH, concentration of the solutions, temperature and stirring speed) must be controlled.

In general, supported Pd-Fe catalysts with a strong metal-metal and/or metal-support interaction can be prepared through the co-precipitation technique [131–139]. As highlighted by Tsang and co-workers [131], it is very important to control pre-reduction treatments, in terms of temperature and duration, because they affect the induction time. Recently, considering the peculiar features of magnetite particles related to their lower sensitivity to oxidation, strong ferromagnetic behavior and easy recovery (aided by an external magnetic field) and reuse, the preparation of Pd/ $\text{Fe}_3\text{O}_4$  catalyst in nanometric scale of different property and composition attracted a lot of interest [196]. Fang and co-workers [197], developed a synthetic route based on the Stöber method and ion-exchange technique to synthesize magnetic core-shell monometallic  $\text{Fe}_3\text{O}_4\text{-SiO}_2/\text{Pd}$  and bimetallic  $\text{Fe}_3\text{O}_4\text{-SiO}_2/\text{Pd-M}$  ( $M = \text{Ag}, \text{Cu}$  and  $\text{Zn}$ ) catalysts at low Pd loading (<0.5 wt %). In this procedure, the syntheses of  $\text{Fe}_3\text{O}_4$  and ferrite microspheres were carried out in a solvothermal system, by modified reduction reactions between  $\text{FeCl}_3$  and ethylene glycol. By the same procedure,  $M\text{Fe}_2\text{O}_4$  ( $M = \text{Co}, \text{Mn}, \text{Zn}$ ) have been prepared in microspheres through co-precipitation [198]. Furthermore, it is possible to adjust the Pd particle size by controlling the shell thickness of the core-shell catalyst. Tsang et al. developed an efficient method based on the addition, at a temperature around 100 °C, of an appropriate additive ( $\text{Zn}^{2+}$  or  $\text{Co}^{2+}$ ) on the support material, which can control—in synergism with Pd particles—the reduction behavior of the supported oxide [132,134].

## 2.2. Physico-Chemical Characterization

The main and most common analysis techniques used so far for the characterization of bimetallic Pd-Fe catalysts are: X-ray Diffraction (XRD), Transmission electron microscopy (TEM), Temperature-programmed reduction ( $\text{H}_2$ -TPR), X-ray photoelectron spectroscopy (XPS) and X-ray absorption fine structure (EXAFS). All these techniques are widely used because they provide accurate results allowing to obtain both quantitative and qualitative results [108].

### 2.2.1. X-ray Diffraction (XRD) and Transmission Electron Microscopy (TEM)

X-ray diffraction (XRD) is a powerful nondestructive structural analysis tool that has been used for decades for characterizing crystalline solids since they contain “matter periodically ordered”.

With respect to heterogeneous catalysts, this characterization technique provides information on: (i) reticular structures; (ii) phases; (iii) texture (preferred crystal orientations) and other important structural parameters including strain crystal size and lattice defects [199,200].

On the other hand, heterogeneous catalysts can be directly examined by transmission electron microscopy (TEM), since it provides most of the necessary fundamental information on morphology and microstructure of the material. Applications of high-resolution TEM to the characterization of heterogeneous catalysts have been largely discussed in the last years [201–204].

X-ray diffraction patterns of impregnated Pd/Fe<sub>2</sub>O<sub>3</sub> and Pd/Fe<sub>3</sub>O<sub>4</sub> and co-precipitated Pd/Fe catalysts, after reduction at 200 °C, are depicted in Figure 3. Diffraction patterns of the impregnated catalysts show peaks related to the metallic Pd species and corresponding support structures Fe<sub>2</sub>O<sub>3</sub> and Fe<sub>3</sub>O<sub>4</sub> [205]. Conversely, co-precipitated Pd/Fe catalysts shows only the Fe<sub>3</sub>O<sub>4</sub> pattern and no peaks related to metallic palladium, indicating the presence of ultra-small palladium particles highly dispersed [128,135,138,206,207]. After 24 h of reaction, no structural modification of the Fe<sub>3</sub>O<sub>4</sub> support was monitored, while the presence of the diffraction peak relative to the (111) plane of the palladium is indicative of Pd particles agglomeration [128].

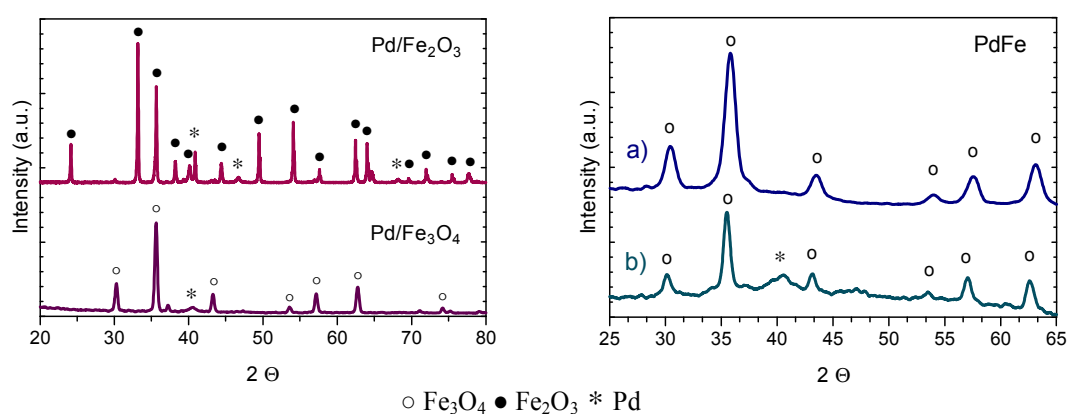


**Figure 3.** X-ray diffraction patterns of impregnated Pd/Fe<sub>2</sub>O<sub>3</sub> and Pd/Fe<sub>3</sub>O<sub>4</sub> catalysts (left side) and co-precipitated PdFe (right side) catalyst before (a) and after (b) 24 h of reaction (adapted from Ref. [129,138]).

TEM and HAADF-STEM of co-precipitated Pd/Fe catalysts allowed to measure the average size of the palladium particles, ranging between 0.5 and 1.5 nm, as depicted in Figure 4 [131].

Tsang et al. synthesized finely dispersed Pd nanoparticles with a proper amount of Fe atoms, controlled through the addition of Zn(II). The average particle size of Pd alloys is nanometric (1–3 nm), indicating that the Zn(II) addition does not influence the particle size [123,132].

Nanometric (1–2 nm) and well dispersed PdFe clusters can be obtained also through the thermal decomposition method, as reported by Braunstein [208].

Wang et al. characterized impregnated monometallic (5Pd/C and 10Fe/C) and bimetallic (2Pd10Fe/C) catalysts supported on carbon [141,209]. STEM-EDS shows, in the bimetallic sample, the presence of PdFe alloys [141,209]. The same authors synthesized Pd/Fe<sub>2</sub>O<sub>3</sub> catalysts through the impregnation technique [142]: XRD patterns evidences the  $\alpha$ -hematite for the iron oxide, whereas Pd is in the metallic form. The presence of Pd does not influence the iron oxide pattern, while lowering the Pd loading (<5 wt %) a high dispersion of the metal is obtained and no characteristic diffraction peaks related to Pd are observed.

Song and co-workers synthesized bimetallic PdFe catalysts supported on OMC (Ordered Mesoporous Carbon), with different Fe/Pd molar ratio (Pd<sub>1</sub>–Fe<sub>X</sub>/OMC, X = 0, 0.25, 0.7, 1.5, 4) [143]. HR-TEM analysis on the reduced catalysts shows that all samples have uniformly dispersed metal particles (average size ca. 4 nm) with pores of OMC support ranging between 4 and 6 nm. STEM-EDX measurements show also the presence of aggregated iron particles on samples having a high Fe/Pd

ratio and formation of a Pd-Fe phase (the remaining part of iron is in the metallic form). XRD patterns of all the catalysts show, together with the characteristic peak of graphitic carbon ( $2\theta = 23.5^\circ$ ) [210], distinctive peaks of palladium, progressively shifted towards higher angle on increasing the Fe/Pd ratio representative of a miscible Pd-Fe phase formation, in which Fe atoms are incorporated into the Pd lattice [211,212].

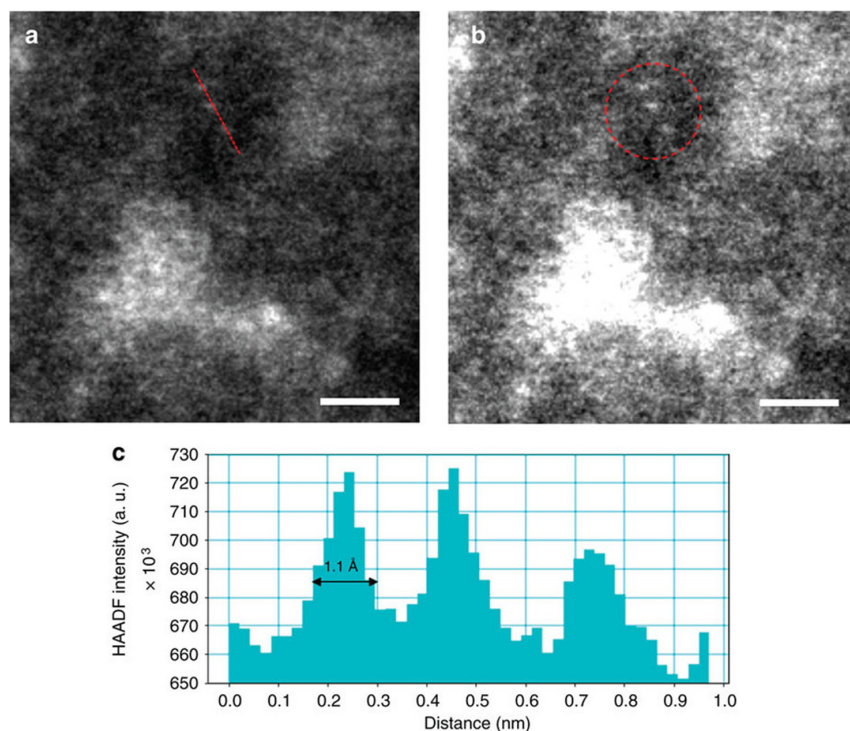


**Figure 4.** HAADF-STEM images of co-precipitated Pd/Fe catalysts (a,b) and the distribution of particle size measured (c) (adapted from Ref. [131]).

### 2.2.2. Hydrogen Temperature-Programmed Reduction ( $H_2$ -TPR)

The hydrogen temperature-programmed reduction ( $H_2$ -TPR) is widely used to find the best reduction conditions for heterogeneous catalysts [213]. The technique consists of heating the sample by a linear temperature ramp in a hydrogen stream, to obtain a fingerprint profile of the sample reducibility that shows the influence of the support and eventual promoters. Furthermore, the amount of hydrogen consumed allows to determine the quantities of reducible species. Consequently, in heterogeneous Pd-Fe catalysts, the  $H_2$ -TPR is a simple and formidable tool to investigate the reduction behavior as well as the interaction between palladium and iron species.

An exhaustive discussion on the  $H_2$ -TPR of bimetallic Pd-Fe catalysts needs to start from the hydrogen-promoted reduction of PdO and  $Fe_2O_3$  oxides.

PdO particles are easily reducible [214], however the reduced palladium crystallites may absorb hydrogen to form two distinctive Pd-H species ( $\alpha$ -PdH if hydrogen is adsorbed only on the surface or  $\beta$ -PdH if hydrogen atoms are absorbed into the bulk). Therefore, the  $H_2$ -TPR profile of Pd-based catalysts may be characterized both by a hydrogen-uptake peak (at lower temperature) and a hydrogen-desorption peak (at higher temperature) [214,215].

On the other hand, the reduction of  $Fe_2O_3$  proceeds in two steps via the  $Fe_3O_4$  intermediate [216,217] as follows: (a)  $3Fe_2O_3 + H_2 \rightarrow 2Fe_3O_4 + H_2O$ ; (b)  $Fe_3O_4 + 4H_2 \rightarrow 3Fe + 4H_2O$ .

The  $H_2$ -TPR analysis of Pd-Fe catalysts supported on OMC was investigated [143] and the results were compared with those obtained with Pd/OMC and Fe/OMC samples (Figure 5, left). Together with a little negative peak at  $60^\circ C$ , relative to Pd-H species, the  $H_2$ -TPR profile of the Pd/OMC

catalyst shows two positive peaks at 172 °C ( $\text{PdO} \rightarrow \text{Pd}$ ) and 591 °C (gasification of the carbon support). The  $\text{H}_2$ -TPR of the Fe/OMC catalyst is characterized by a broad reduction peak that, after deconvolution, can be related to successive reductions of  $\text{Fe}_2\text{O}_3$  to  $\text{Fe}_3\text{O}_4$  at 335 °C,  $\text{Fe}_3\text{O}_4$  to FeO at 496 °C and FeO to Fe(0) at 561 °C. Conversely, the profile of bimetallic Pd-Fe/OMC catalyst, shows a broad and intense peak related to the simultaneous reduction of both Pd and Fe cations suggesting that: (i) Pd nanoparticles increase the reducibility of Fe species and (ii) the addition of Fe inhibits formation of palladium hydride species. The same authors investigated analogous Pd-Fe based catalysts with different Pd/Fe composition [144]. By increasing the Fe content, the  $\text{H}_2$ -TPR broad peak moves toward higher temperature clearly indicating that the bimetallic phase can be tuned by an opportune Pd/Fe ratio.

The difference in temperature profiles of hydrogen consumption, relative to impregnated Pd/ $\text{Fe}_2\text{O}_3$  and Pd/ $\text{Fe}_3\text{O}_4$  catalysts, compared with the co-precipitated Pd/Fe sample, was deeply investigated by Pietropaolo and Mauriello (Figure 5, right) [135,138,193]. In impregnated Pd/ $\text{Fe}_2\text{O}_3$  and Pd/ $\text{Fe}_3\text{O}_4$  catalyst a modest interaction between palladium and supports is observed. Conversely, the  $\text{H}_2$ -TPR profile of the coprecipitated Pd/Fe catalyst, characterized by one reaction area relative to both  $\text{Pd}^{2+} \rightarrow \text{Pd}^0$  and  $\text{Fe}^{3+} \rightarrow \text{Fe}_3\text{O}_4$  reductions, is indicative of a strong metal-support interaction (SMSI).

The same conclusions were drawn by other authors on the  $\text{H}_2$ -TPR analysis of various heterogeneous Pd-Fe catalysts, that all agree on the promoting effect of Pd nanoparticles in the reduction of support [128,131–134,138]. On this regard, Asakura remarks that Pd nanoparticles can produce hydrogen-spillover onto the Fe oxide surface [138]; Qiao suggests that the promoting effect of Pd in the reduction of hematite to magnetite derives directly from the catalyst preparation method (co-precipitation) [128]; while Tsang highlights that the reduction of the iron support can be further promoted by the assistance of Zn(II) nanoparticles in co-precipitated Pd/Fe catalysts blended with Zn(II) [132,133].

The enhanced  $\text{Fe}_2\text{O}_3$  reducibility via surface modification with palladium was also investigated by McEwen and co-workers with a combined experimental and theoretical studies [209]. DFT calculations coupled with XPS analysis show that Pd is able to partially donate electrons to the topmost surface Fe, allowing the oxide surface electrons to become more delocalized than in pure  $\text{Fe}_2\text{O}_3$ . Most important, the presence of palladium prevents oxygen poisoning effects on the active metallic Fe, facilitating the reduction of  $\text{FeO}_x$  species and promoting the formation of water.

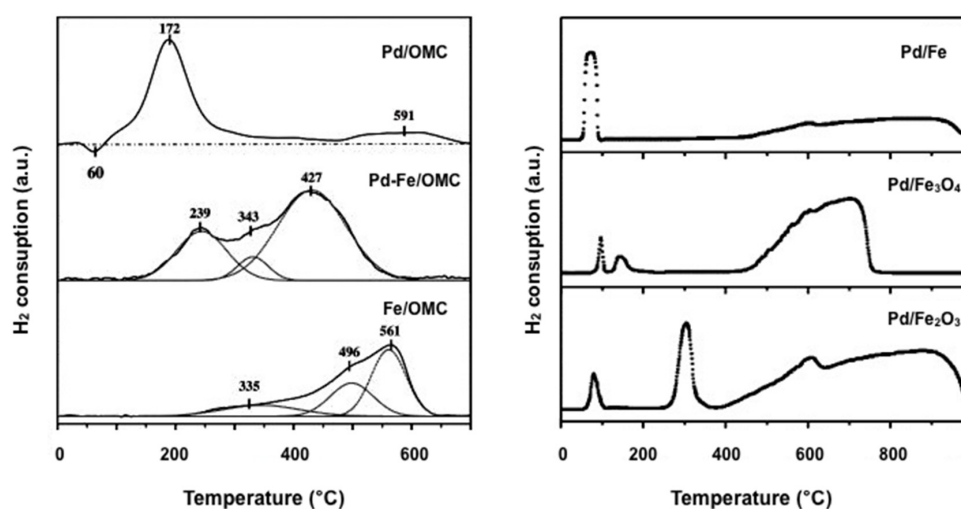


**Figure 5.**  $\text{H}_2$ -TPR profiles of Pd/OMC, Pd-Fe/OMC, Fe/OMC (left) and Pd/Fe, Pd/ $\text{Fe}_3\text{O}_4$  and Pd/ $\text{Fe}_2\text{O}_3$  catalysts (right) (adapted from Ref. [138,143]).

### 2.2.3. X-ray Photoelectron Spectroscopy (XPS)

X-ray photoelectron spectroscopy (XPS) allows to study the materials surface, permitting to know the chemical composition and to establish the involved bonds [218–220]. It consists in the irradiation of a sample with a monochromatic x-ray source: photons enter the material and undergo various interactions, leading to the photoelectric effect and the Auger emission. In both cases, an electron is ejected from the material with a given kinetic energy that allows information on energies involved on internal electrons of the case materials.

Table 1 shows XPS data for a series of heterogeneous Pd-Fe bimetallic catalysts.

**Table 1.** XPS data for a series of heterogeneous Pd-Fe based catalysts.

Catalyst Notation	Preparation Method <sup>1</sup>	Binding Energy (eV)				References
		Pd 3d <sub>5/2</sub>	Fe 2p <sub>3/2</sub>	Fe 2p <sub>1/2</sub>	Fe 2p <sub>3/2</sub> <sup>sat</sup>	
Pd/Fe	CP	335.2 ± 1	710.7 ± 0.8	724.4	-	[131,135,137–139]
Pd-rod Fe <sub>2</sub> O <sub>3</sub>	DP	335.9	711.2	-	-	[134]
Pd-plate Fe <sub>2</sub> O <sub>3</sub>	DP	335.7	711.4	-	-	[134]
PdCo/Fe <sub>2</sub> O <sub>3</sub>	CP	334.8	710.2	-	-	[133]
Pd-Zn/Fe <sub>2</sub> O <sub>3</sub>	CP	334.8	707.8	-	-	[132]
Pd/Fe <sub>2</sub> O <sub>3</sub>	IWi	334.8	710.4	723.8	718.4	[135,138,142]
Pd/Fe <sub>3</sub> O <sub>4</sub>	IWi	334.8	710.5	-	-	[138]
Pd-Fe/OMC	IWi	334.4	708.2	-	-	[143]
Pd <sub>1</sub> -Fe <sub>x</sub> /OMC	IWi	334.4	708.2	-	-	[144]

<sup>1</sup> CP = Coprecipitation; DP = Deposition; IWi = Impregnation.

XPS analysis of the heterogeneous Pd-Fe catalysts shows that the binding energy for Pd 3d<sub>5/2</sub> level is generally different than that measured in the monometallic Pd-based catalyst, suggesting that the electronic property of Pd can be easily modified by addition of Fe atoms [131,138].

It is noticeable that the preparation method affects the final electronic properties of the catalysts. Indeed, the binding energy value of 334.8 eV relative to the Pd 3d<sub>5/2</sub> for impregnated Pd/Fe<sub>2</sub>O<sub>3</sub> and Pd/Fe<sub>3</sub>O<sub>4</sub> samples, indicates the presence of metallic palladium and no evidence of surface Pd-Fe interaction [135,138,193]. The co-precipitated Pd/Fe catalyst, after H<sub>2</sub> reduction at 200 °C, shows a binding energy value relative to the Pd 3d<sub>5/2</sub> level of about 0.4 eV higher than that of analogous catalysts prepared by IWi [135,138,193] that can be assigned to Pd-Fe alloy formation. Moreover, by adding a second co-metal (Zn), it was demonstrated that both positions of the d-band filling and d-band center of Pd and Fe may be opportunely adjusted [132].

On the other hand, XPS analysis of the Fe 2p and O 1s regions shows a modest “blue” shift (ca. 0.1 eV for Fe and 0.2 eV for O) indicating that: (i) Fe has a higher electron affinity and (ii) the electron status of oxygen is modified by addition of Pd. Indeed, a decrease of the binding energy values for the (Fe 2p<sub>3/2</sub>) to 710.2 and 707.8 eV for PdCo/Fe<sub>2</sub>O<sub>3</sub> and PdZn/Fe<sub>2</sub>O<sub>3</sub>, respectively, have been reported [132,133]. These results suggest that blending Co (II) or Zn (II) into the Fe<sub>2</sub>O<sub>3</sub> support of precipitated PdO-Fe catalysts leads to a further reduction of Fe ions during the hydrogen reduction treatment.

### 2.2.4. Extended X-ray Absorption Fine Structure (EXAFS)

Extended X-ray absorption fine structure (EXAFS) can provide valuable information about the structure of metal alloys, since it is the only spectroscopic technique that gives information on the local structure around Pd, the Pd-support oxide interaction and/or the Pd bimetal nanoparticle formation [221–223].

EXAFS characterization on different co-precipitated Pd/Fe<sub>2</sub>O<sub>3</sub> catalysts has been deeply investigated by the research group of Prof. Tsang [109,131–134]. The motivation beyond the use of EXAFS spectroscopy needs to be found in the necessity to define both the dimension of Pd nanoparticles (too small to be accurately detected by classic XRD and TEM analysis) as well as to confirm the presence

of Pd-Fe bimetallic clusters on the catalyst surface (as suggested by XPS measurements). EXAFS analysis reveals Pd particles smaller than 1 nm well-dispersed into the iron oxide support and the presence of Pd-Fe bimetallic clusters. The shorter Pd-Fe distance can be ascribed to the smaller size of Fe than that of Pd.

Results similar to those obtained by Tsang and co-workers were obtained by other authors (Table 2). Wang et al. coupled EXAFS analysis with DFT calculations to better understand the interaction between Pd and Fe nanoparticles on the 2Pd10Fe/C catalyst [141]. Two scenarios were investigated: the first with a top pure Pd layer on the surface of the Fe (110) host and the other with a Fe layer within the Pd(111) surface host. Theoretical calculations suggest that the surface of the Pd-Fe alloy is enriched in Pd while the subsurface is widely featured by metallic Fe.

**Table 2.** Extended X-ray adsorption fine structure (EXAFS) analysis for Pd K-edge of commercial Pd/C and different coprecipitated Pd-Fe based catalysts.

Catalyst Notation	Scattering Pair	CN *	Bond Length (Å)	R-Factor (%)	Ef (eV)	DW Factor ** (Å <sup>2</sup> )	k-Range	References
Pd/C	Pd-Pd	8.0 (3)	2.73 (1)	2.6	-7.6	6.1 (3)	2-17	[131]
Pd/Fe <sub>2</sub> O <sub>3</sub> (before reduction)	Pd-O	3.5 (2)	2.01 (1)	1.3	-4.5	2.8 (6)	2-16	[131]
Pd/Fe <sub>2</sub> O <sub>3</sub> (after reduction)	Pd-Fe	1.0 (2)	2.59 (1)			5.1 (4)		
	Pd-Pd	1.9 (2)	2.66 (1)	1.6	-7.4	7.3 (6)	2-12	[131]
	Pd-Pd	2.4 (2)	2.75 (1)			3.6 (3)		
Pd-Co/Fe <sub>2</sub> O <sub>3</sub>	Pd-Pd	6.8 (4)	2.69 (1)	0.4	1.2	0.010 (1)	-	[133]

\* CN = coordination number; \*\* DW = Debye Waller (numbers in parentheses indicate the statistical error in the most significant digit obtained from the first Artemis).

### 3. Hydrogenolysis Reactions of Biomass-Derived Platform Molecules Promoted by Heterogeneous Pd-Fe Catalysts

#### 3.1. Valorization of Cellulose and Hemicellulose Derived Molecules

##### 3.1.1. C-C and C-O Bond Breaking in C<sub>2</sub>-C<sub>6</sub> Polyols

Cellulose deriving polyols are characterized by the highest O/C ratio than other biomass-derived molecules and typical chemical commodities and fuels available in the industrial market. Therefore, the main issue consists in reducing the oxygen content through deoxygenative and CTH/APR processes [224-229].

Ethylene glycol [227] (EG) is the simplest basic unit of polyols and can be used as representative for larger polyols and sugars molecules to exploit the selective cleavage of C-C, C-H, O-H and C-O bonds. Currently, EG is mainly produced via ethylene by cracking of fossil raw materials, but can be also easily obtained from the direct catalytic conversion of cellulosic biomass [228,229].

Bond energies of both C-C and C-OH bonds are almost the same ( $\Delta H_{C-C}$  83 kcal·mol<sup>-1</sup> and ( $\Delta H_{C-O}$  86 kcal·mol<sup>-1</sup>) [230,231], therefore, on performing the reaction under drastic operating conditions, it is less likely to achieve a higher selectivity. If hydrogenolysis breaks selectively C-C bond, methanol will be the favourite reaction product; on the contrary, the breaking of the C-O bond will generate ethanol, that can be further converted into CO<sub>2</sub> or CH<sub>4</sub> (Figure 6) [129].

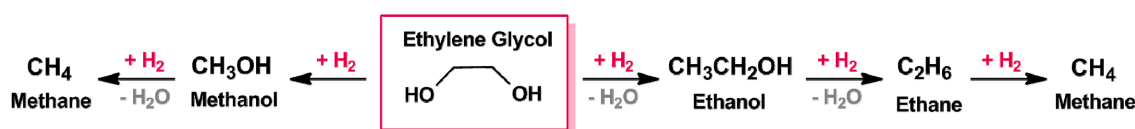


**Figure 6.** Hydrogenolysis of ethylene glycol.

Tsang and co-workers successfully used the co-precipitated Pd/Fe<sub>2</sub>O<sub>3</sub> catalyst for methanol production from ethylene glycol [131]. The peculiar reactivity of the catalyst, after reduction, was

conferred by the strong metal-support interaction exerted through the extremely small PdFe clusters. Hydrogenolysis of EG, on 5% Pd/Fe<sub>2</sub>O<sub>3</sub> catalyst at 195 °C and 20 bars of hydrogen, denoted high selectivity to the methanol and ethanol mixture. Other metal particles (Ru) and different oxide supports (ZnO, Ga<sub>2</sub>O<sub>3</sub>, CeO<sub>2</sub> and Al<sub>2</sub>O<sub>3</sub>) were tested: the only combination for a good methanol production was found to be Pd and iron oxide (Figure 7b).

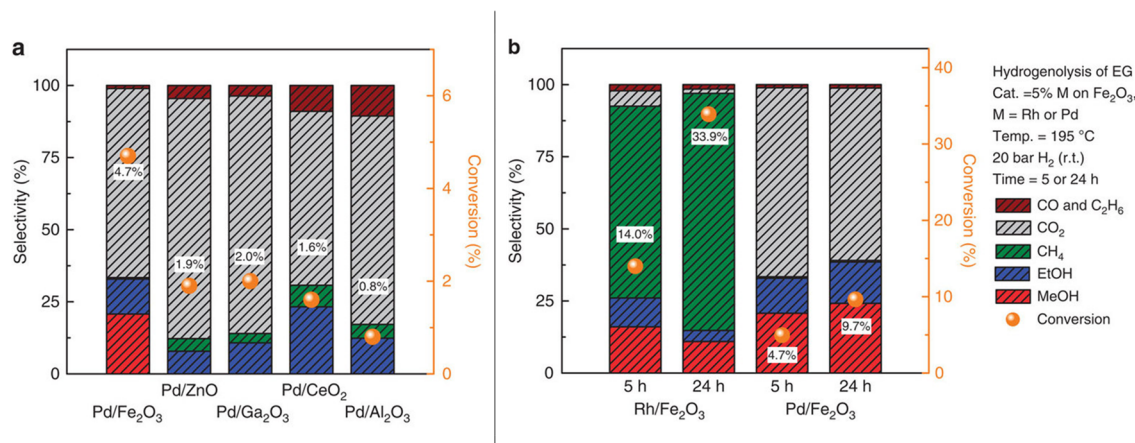


**Figure 7.** Hydrogenolysis of EG promoted by (a) 5% Pd supported on different oxides and (b) by 5% Pd and 5% Rh supported on iron oxide (adapted from Ref. [131]).

Bimetallic PdM (M = Fe, Co, Zn) samples were investigated in the hydrogenolysis of EG to explore the effect of the d-band filling parameter on the cleavage of C–O and C–C bonds [133]. As illustrated in Figure 8, experimental results show a significant decrease of the selectivity to methanol from 50.1% with the PdFe sample to 18.6% with the PdZn system. On the contrary, the selectivity to ethanol increases on passing from a value of 3% to 23.6%.

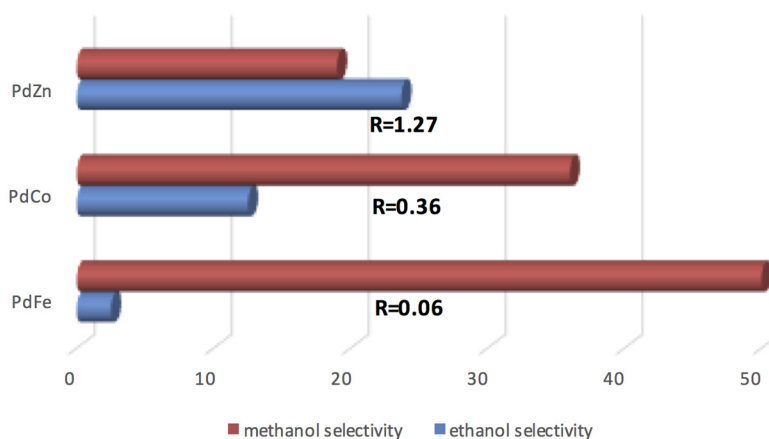


**Figure 8.** Hydrogenolysis of EG on PdFe, PdCo and PdZn catalysts. R = the molar ratio C–O/C–C bond breakage (adapted from Ref. [133]).

A series of heterogeneous Pd-Fe catalysts blended with diverse concentrations of Zn(II) were also prepared and tested in the EG hydrogenolysis [132]. A significant selectivity toward the C–C bond cleavage was registered, related to the increased amount of neighbor Fe atoms in the PdFe nanoclusters (Figure 9). Furthermore, the C–C bond breaking ability increases almost linearly with the concentration of Fe(0) present in the catalytic system.

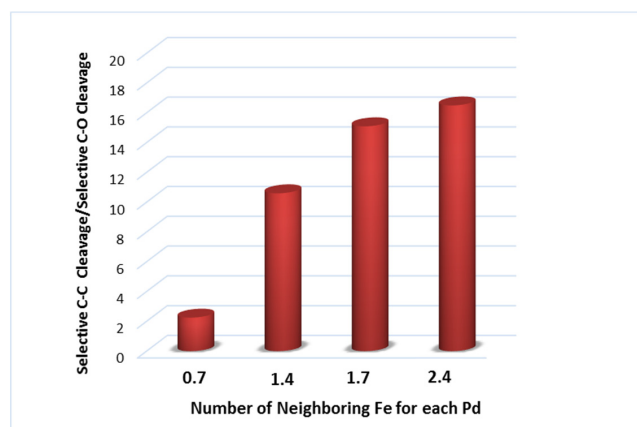


**Figure 9.** Relationship between the selectivity in C–C bond cleavage obtained in hydrogenolysis of EG and the Fe content in Pd-Fe (adapted from Ref. [132]).

Mauriello et al. studied the performance of the 5% Pd/Fe<sub>3</sub>O<sub>4</sub> co-precipitated catalyst in the hydrogenolysis of EG [129]. At low temperature (180 °C), the Pd/Fe<sub>3</sub>O<sub>4</sub> system shows nearly the same selectivity to methanol (49.9%) and ethanol (50.1%). Upon raising the reaction temperature, the EG conversion increases up to 72.1% at 240 °C with a methanol selectivity of 76.6% [129]. Simulating APR conditions, the conversion of EG was carried out under identical reaction conditions without added H<sub>2</sub>. The same performance obtained in presence of molecular hydrogen was observed with the gas phase mainly composed by H<sub>2</sub> (81%–82%), followed by CO<sub>2</sub> (about 18%). CO was never detected indicating the high performance of the Pd/Fe<sub>3</sub>O<sub>4</sub> toward the water-gas-shift reaction [129].

Dumesic and co-workers were pioneers in developing the aqueous-phase reforming (APR) process from oxygenated molecules [75–86]. Bimetallic Pd-Fe catalytic systems were investigated for APR of EG [79]. Authors highlight the promoting effect of iron in the APR process, giving a significant improvement in TOF related to H<sub>2</sub> production, with the 6% Pd/Fe<sub>2</sub>O<sub>3</sub> sample being considered the most promising catalytic system.

The real potential of Pd/Fe<sub>3</sub>O<sub>4</sub> in APR of biomass-derived oxygenated molecules was sustained and confirmed also by Qiao [128]. Pd-based catalysts were prepared by IWi over different metal oxide supports (Fe<sub>2</sub>O<sub>3</sub>, Cr<sub>2</sub>O<sub>3</sub>, NiO, Al<sub>2</sub>O<sub>3</sub>, ZrO<sub>2</sub>). Pd/Fe<sub>2</sub>O<sub>3</sub> appears as the most suitable IWi catalyst for its superior activity, selectivity and stability in APR of EG. Moreover, the Pd/Fe<sub>3</sub>O<sub>4</sub> catalyst—prepared through co-precipitation—shows superior performance than those obtained with the impregnated Pd/Fe<sub>2</sub>O<sub>3</sub> sample, while the H<sub>2</sub> selectivity remains on the same order of magnitude (94.2%), confirming the importance of the preparation method used [128].

Glycerol (C3 polyol), the main by-product obtained from the biodiesel production, is gaining importance as bio-feedstock to produce chemicals, because of the growing worldwide expansion of biofuels [31–33]. An attractive valorization route is the selective hydrogenolysis of glycerol because it is a clean and economically competitive process that allows production of different valuable chemicals such as 1,2-propanediol (1,2-PDO), 1,3-propanediol (1,3-PDO), ethylene glycol (EG) and C1–C3 alcohols [34]. Great efforts have been focused on its conversion into 1,2-PDO that is widely used in the manufacture of pharmaceuticals, cosmetics, food products, polyester resins and functional fluids. Moreover, glycerol can be used as starting substrate for the sustainable production of renewable hydrogen through the APR process.

The performance of bimetallic PdFe catalysts on glycerol hydrogenolysis was recently investigated to ascertain the morphological effect of the iron oxide support (rod-like and plate-like) on the catalyst activity [134]. Pd-plate-like iron oxide catalysts show higher activity than Pd-rod-like samples with the glycerol conversion/1,2-PDO production increasing with the reduction temperature (200–300 °C) [232,233]. The higher activity shown by the Pd-plate-like iron oxide catalyst was correlated to a higher amount of active sites at the interface [234,235]. Moreover, CO<sub>2</sub>-TPD measurements reveal an exact correlation



On the bimetallic Pd-Fe catalytic system, the hydrogenolysis of glycerol can follow two main initial routes, reported in Figure 11 [129]: (i) the dehydration/hydrogenation route that implies the breaking of the C–O bond leading to 1,2-PDO production or (ii) the dehydrogenation/decarbonylation route, where the breaking of the C–C bond allows the EG formation. Dehydration and dehydrogenation reactions were found to be key elementary steps both in the presence and in absence of H<sub>2</sub>; their selectivity is driven by the reaction temperature effect on the selective cleavage of bonds involved. The dehydration/hydrogenation route easier occurs at lower temperature since the initial C–OH breaking involves an energy bond as low as  $\cong 80 \text{ kcal}\cdot\text{mol}^{-1}$ , while the dehydrogenation/decarbonylation preferentially proceeds at higher temperature since the cleavage of the O–H bond implies a much higher energy value ( $E_{\text{O-H}} \cong 104 \text{ kcal}\cdot\text{mol}^{-1}$ ) [230].

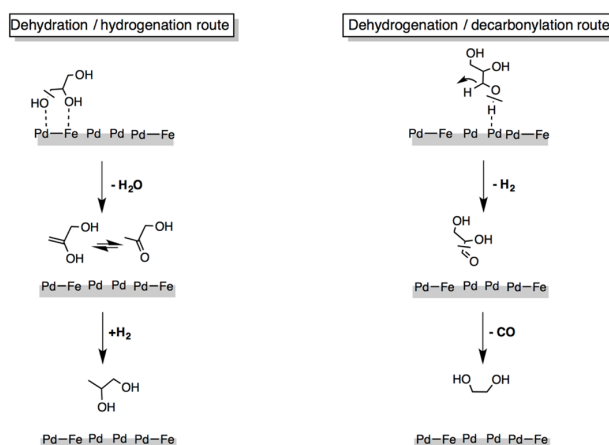


**Figure 11.** Main pathways of glycerol hydrogenolysis over Pd/Fe catalyst (adapted from Ref. [129]).

The effective feasibility of the selective catalytic transfer hydrogenolysis of glycerol into 1,2-PDO, promoted by the PdFe catalyst, was demonstrated for the first time by Pietropaolo [137]. Reactions were performed under inert atmosphere in absence of added hydrogen and it was ascertained that the transfer of hydrogen occurs from the alcoholic solvent (2-propanol or ethanol) to the glycerol, through the dehydrogenation of the solvent. Glycerol hydrogenolysis reactions were carried out within 24 h in an autoclave charged with 5 bar of inert gas, using PdO/Fe<sub>2</sub>O<sub>3</sub> unreduced catalyst and a glycerol (12 wt %) solution in 2-propanol (or ethanol). The glycerol reaches the complete conversion (84%–100%) in the temperature range of 150–180 °C, showing a remarkable selectivity to 1,2-PDO (91%–94%), followed by a minor amount of ethylene glycol (EG). Acetone was also detected in liquid phase, being produced from the 2-propanol dehydrogenation. The presence of 1-hydroxyacetone (AC) is an important intermediate, that enables to maximize the selectivity to 1,2-PDO and it was detected in reactions carried out in a shorter time than 24 h.

Glycerol CTH reactions under mild conditions (180 °C, 5 bar of N<sub>2</sub>), in 2-propanol as solvent, were deeply investigated to understand the different reactivity obtained from co-precipitated and impregnated PdFe catalysts [138]. Impregnated samples (Pd/Fe<sub>2</sub>O<sub>3</sub> and Pd/Fe<sub>3</sub>O<sub>4</sub>) result considerably less active than the analogous co-precipitated, and AC was detected as the prevalent product, followed by 1,2-PDO and EG in small percentages. An interesting correlation between the amount of acetone measured and the glycerol conversion was also experimentally verified. A reaction mechanism of glycerol in CTH condition was proposed. The first step involves the glycerol chemisorptions on metal sites. The following C–OH cleavage occurs through a S<sub>N</sub>1 mechanism with an internal re-arrangement into acetol. Finally, the transfer hydrogenation of acetol to 1,2-PDO occurs directly from 2-propanol or through the H-species obtained from the dehydrogenation of 2-propanol [138].

The main results discussed for hydrogenolysis, APR and CTH reactions of glycerol are reported in Table 3.

**Table 3.** Catalytic conversion of glycerol in hydrogenolysis, APR and CTH conditions over PdFe catalysts.

Catalyst	Preparation Method <sup>1</sup>	Substrate [wt %] <sup>2</sup>	Solvent	H-Source	Temp. [°C]	Time [h]	Conversion [%]	Main Products [%] <sup>4</sup>	References
Zn-Pd/Fe <sub>3</sub> O <sub>4</sub>	CP	Gly (1%)	H <sub>2</sub> O	H <sub>2</sub> (50 bar)	250	120	100	1,2-PDO (33%), EtOH (32%)	[132]
Pd/Fe <sub>3</sub> O <sub>4</sub>	CP	Gly (1%)	H <sub>2</sub> O	H <sub>2</sub> (50 bar)	250	120	100	1,2-PDO (36%), EtOH (17%), 1-PO (15%)	[132]
Pd/Fe <sub>3</sub> O <sub>4</sub>	CP	Gly (4%)	H <sub>2</sub> O	H <sub>2</sub> (5 bar)	240	24	100	EtOH (70%), POs (10%)	[129]
Pd/Fe <sub>3</sub> O <sub>4</sub>	CP	Gly (4%)	H <sub>2</sub> O	APR (5bar)	240	24	100	EtOH (73%), 1,2-PDO (9.4%)POs (8.7%)	[129]
PdO/Fe <sub>2</sub> O <sub>3</sub>	CP	Gly (12%)	2-PO <sup>3</sup>	2-PO (5bar)	180	24	100	1,2-PDO (94%), EG (6%)	[137]
Pd/Fe <sub>3</sub> O <sub>4</sub>	CP	Gly (4%)	2-PO	2-PO (5bar)	180	24	100	1,2-PDO (56%), AC (25%)	[138]
Pd/Fe <sub>3</sub> O <sub>4</sub>	IWi	Gly (4%)	2-PO	2-PO (5bar)	180	24	66.5	1,2-PDO (48%), AC (44%)	[138]
Pd/Fe <sub>2</sub> O <sub>3</sub>	IWi	Gly (4%)	2-PO	2-PO (5bar)	180	24	40.4	1,2-PDO (26.6%), AC (58%)	[138]

<sup>1</sup> CP: coprecipitation; IWi: incipient wetness impregnation; <sup>2</sup> Gly: glycerol; <sup>3</sup> 2-PO: 2-propanol; <sup>4</sup> 1,2-PDO: 1,2-propanediol; EtOH: ethanol; EG: ethylene glycol; AC: 1-hydroxyacetone.

Considerable research interest has been directed towards sorbitol (C6 polyol) hydrogenolysis, because it allows the production of fundamental chemical intermediates [68,241–243].

The overall reaction pathway of sorbitol hydrodeoxygenation is reported in Figure 12 [244]. The sorbitol conversion mainly exhibits four key reactions: hydrogenation, dehydration, retro-aldol condensation and decarbonylation [245]. Sorbitol could be dehydrated to cyclic products such as 1,4-sorbitan and isosorbide. The latter leads to 1,2,6-hexanetriol (1,2,6-HXT) through hydrogenolysis and dehydration/hydrogenation reactions. 1,2,6-HXT is a valuable intermediate because, through dehydration/decarbonylation reactions, affords lighter alcohols and polyols; alternatively, it could be dehydrated and hydrogenated to hexanol. Hexanols can be converted into alkanes, like *n*-pentane and *n*-hexane through dehydrogenation/decarbonylation or dehydration/hydrogenation, respectively. Most of the C4 and C5 oxygenates are obtained by decarbonylation reactions and can be converted into alkanes (*n*-butane and *n*-pentane) or into shorter oxygenates and alkanes through decarbonylation reactions. The retro-aldol condensation of sorbitol leads to C2 and C3 alcohols and polyols, that are further converted into alcohols or alkanes by dehydration and hydrogenation reactions [245]. As a whole, the conversion of sorbitol mainly involves (i) the cleavage of the C–OH group through dehydrogenation/decarbonylation; (ii) the C–C bond breaking by retro-aldol condensation or (iii) the C–H and C–OH cleavage through the dehydration/hydrogenation route.

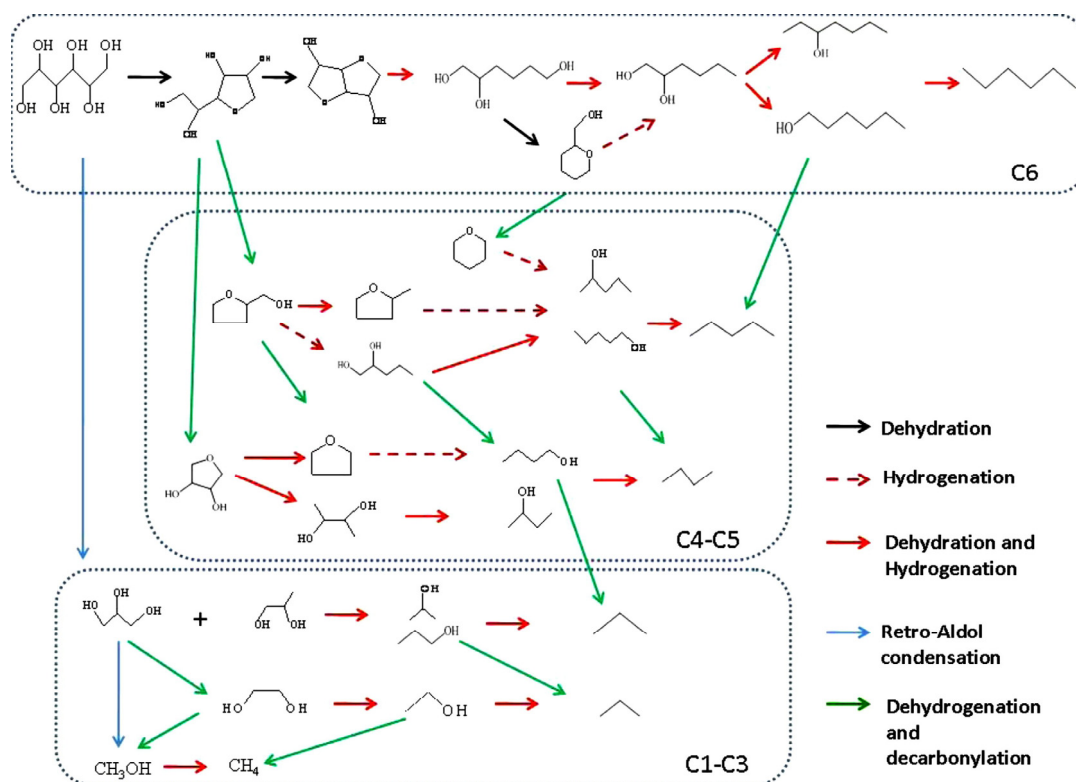


Figure 12. Reaction network in the HDO of sorbitol (Ref. [200]).

Dumesic and co-workers demonstrated, for the first time, that sorbitol can be hydrodeoxygenated to alkanes over a series of noble metal loaded over solid acid catalysts [75,76]. Zr-P is a promising solid-acid support for the HDO process, because it is stable in hydrothermal conditions, does not give leaching problems and has more Brønsted acid sites than Lewis sites [140]. The addition of Fe to Pd appears a useful way to improve the catalytic activity. Indeed, the Pd<sub>1</sub>Fe<sub>3</sub> sample supported on zirconia phosphate (Zr-P) shows a significant activity compared to other catalysts screened. A previous analysis showed that Fe addition to Pd plays a positive role, improving the activity up to 63 times for the hydrogenation of the carbonyl group, that is a fundamental step in

HDO of biomass-derived oxygenated molecules [244,246,247]. As shown in Figure 13, the bimetallic Pd<sub>1</sub>Fe<sub>3</sub>/Zr-P affords the highest activity than other screened catalysts [140,248]. The authors reported the detailed product selectivity concerning 3 wt % Pd/Zr-P and Pd<sub>1</sub>Fe<sub>3</sub>/Zr-P catalysts, grouped by product functionality [140]. More C1–C4 products are formed upon adding Fe to Pd catalysts [248]. This stems from the higher amount of Fe-containing bimetallic sites [249].

Moreover, the Pd<sub>1</sub>Fe<sub>3</sub>/Zr-P shows a lower selectivity toward dehydration products (sorbitan and isosorbide). This means that the bimetallic catalyst promotes subsequent hydrogenolysis reactions of sorbitan and isosorbide through a series of dehydration/hydrogenation steps. Also in this case, the ability of the Pd/Fe system to avoid undesired side reactions, such as methanation or methane reforming was confirmed [250–252]. For a high conversion value (WHSV 0.16 h<sup>-1</sup>), the presence of humins, derived from polymerization of isosorbide, was noticed [253].

In the presence of the Pd<sub>1</sub>Fe<sub>3</sub>/Zr-P catalyst a product mixture with an octane number (101.3) higher than that of the Pd/Zr-P (92.2) was obtained. The bimetallic system was found more selective in affording gasoline-range products, showing a higher yield (55.1%) than that of the Pd/Zr-P substrate (24.1%).

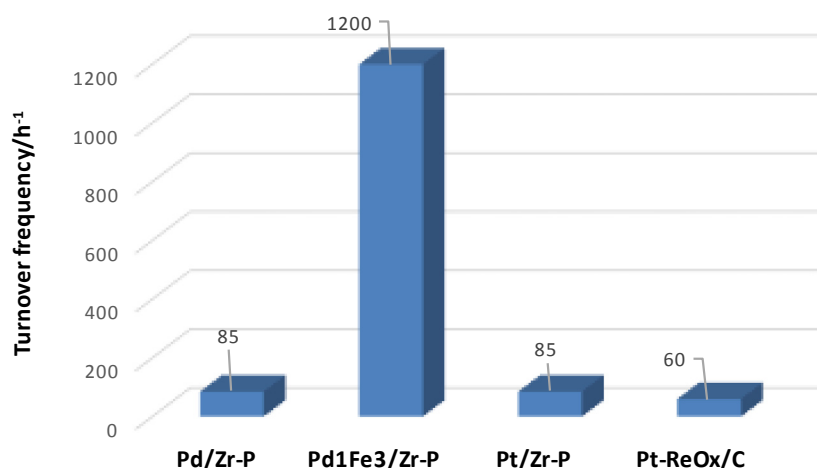


**Figure 13.** Comparison of TOF in HDO of sorbitol over Pd- and Pt-based catalysts (adapted from Ref. [140]).

### 3.1.2. Hydrogenation/Hydrogenolysis of Furfural and 5-Hydroxymethylfurfural

Furfural and 5-hydroxymethylfurfural (HMF) are easily obtained from hemicellulose and cellulose [254–256]. The sequential hydrogenation/hydrogenolysis of furfural allows the production of furfuryl alcohol (FA) that can be transformed into 2-methylfuran (MeF) through the successive hydrogenolysis of the OH group (Figure 14).

The CTH of furfural and 5-hydroxymethylfurfural was investigated over co-precipitated Cu, Ni, and Pd based Fe<sub>2</sub>O<sub>3</sub> catalysts using 2-propanol as H-source [139]. The main product, for all tested catalysts, was FA with Pd/Fe<sub>2</sub>O<sub>3</sub> exhibiting a higher activity in the production of MeF. The different activities of the co-precipitated catalysts were correlated to the degree of reduction reached, with H<sub>2</sub>-TPR analysis clearly indicating that complete reduction of metallic species is observed only in the case of supported Pd samples. The authors investigated the reactivity of Pd/Fe<sub>2</sub>O<sub>3</sub> catalysts with different palladium loadings (2, 5, and 10 wt %). 2 wt % Pd/Fe<sub>2</sub>O<sub>3</sub> shows the highest activity in the catalytic transfer hydrogenation that can be related to a better interaction, at that metal loading, between Pd and Fe species that lets an easily O–H bond activation.

The authors investigated also the CTH of FA. Cu/Fe<sub>2</sub>O<sub>3</sub> and Ni/Fe<sub>2</sub>O<sub>3</sub> show limited-to-no activity while on Pd/Fe<sub>2</sub>O<sub>3</sub> catalysts, THFA, MeF, and THMeF are formed. Accordingly, the low activity observed with other Pd-based catalysts (Pd/C, Pd/MgO, and Pd/Al<sub>2</sub>O<sub>3</sub>) further confirms that the higher reactivity obtained with Pd/Fe<sub>2</sub>O<sub>3</sub> can be related to the SMSI effect.

The aqueous-phase hydrogenation (APH) of furfural, xylose and propanal was investigated on Pd-Fe/Al<sub>2</sub>O<sub>3</sub> catalysts [140]. The addition of Fe increases the catalytic activity of the system suggesting that the presence of Fe in the Pd-Fe bimetallic surface decreases the fermi level, allowing an easier hydrogenation of the C=O group [257,258].

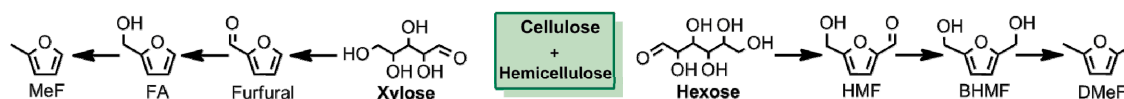


**Figure 14.** Sequential hydrogenation/hydrogenolysis of furfural and 5-hydroxymethylfurfural (adapted from Ref. [139]).

### 3.2. Valorization of Lignin Model Molecules

#### 3.2.1. Hydrodeoxygenation of Phenol Derivatives

Degradation of lignin generates a significant amount of oxygen-rich phenolic compounds [259–261]. With respect to other hydrodeoxygenation process [262,263], the cleavage of the aromatic C–O bond requires a dissociation energy of about 100 kJ/mol higher than those of the corresponding aliphatic bond [192], even if the latter is generally characterized by lower steric constraints. It is therefore highly important to understand the integrated steps of hydrogenolysis, hydrogenation, hydrolysis, and dehydration reactions [264] to selectively cleave the different bonds present in lignin model molecules.

Guaiaicol (2-methoxyphenol) has attracted a lot of interest since it is characterized by two distinctive oxygenated groups (phenolic and methoxy functionalities). Hydrogenolysis of guaiaicol was reported to follow two possible reaction pathways (Figure 15) [141,265]. In the first reaction sequence, guaiaicol is first converted to methane and catechol. Catechol is further converted into phenol via hydrogenolysis of the hydroxyl group. Alternatively, guaiaicol can be directly converted into phenol via hydrogenolysis of the methoxy group. Finally, phenol may undergo sequential hydrogenolysis and hydrogenation reactions forming benzene, cyclohexanone, and cyclohexanol. Finally, phenol may undergo sequential hydrogenolysis and hydrogenation reactions forming benzene, cyclohexanone, and cyclohexanol. Finally, phenol may undergo sequential hydrogenolysis and hydrogenation reactions forming benzene, cyclohexanone, and cyclohexanol. Finally, phenol may undergo sequential hydrogenolysis and hydrogenation reactions forming benzene, cyclohexanone, and cyclohexanol.

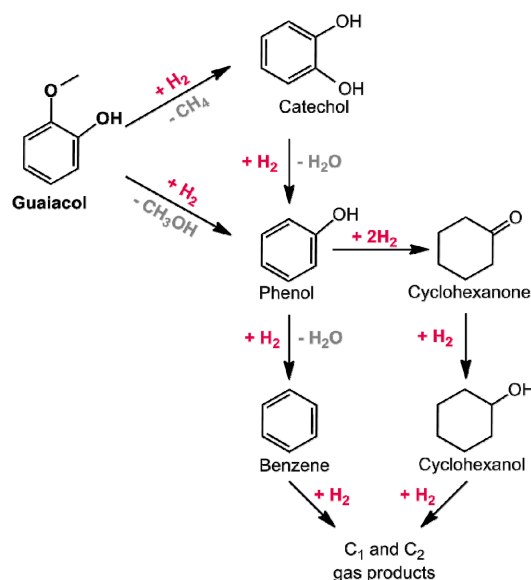


**Figure 15.** Reaction pathways observed in guaiaicol HDO (adapted from Ref. [141]).

Under atmospheric pressure, precious metal catalysts show higher activity in the hydrogenolysis of guaiaicol with phenol, being the major reaction intermediate [141]. However, aromatic ring hydrogenation and C–C bond breaking was always observed leading to formation of cyclohexanone,

cyclohexanol, and gaseous products. Metallic iron is a good catalyst for the HDO of guaiacol avoiding, at the same time, the ring-saturation side reaction. However, the Fe/C activity was lower than that observed with carbon-supported precious metals. Therefore, to further improve the activity of the Fe catalyst, a Pd-Fe/C catalyst (Pd 2%-Fe 10%) was tested. Guaiacol is fully deoxygenated on the Pd-Fe/C, at 450 °C, with a high yield to BEX (83.2%).

The adsorption of phenol on the Pd-Fe surface was investigated by DFT calculations. As the distance increases, both the adsorption energy and the carbon–oxygen bond length increase, suggesting that phenol adsorption is more favorable on the Fe surface. The presence of palladium facilitates the reduction of iron-oxide and modifies the Fe surface, leading to the enhanced HDO of phenol. The absence of ring saturation on the PdFe/C catalyst was explained, on the basis of DFT calculations, with the preferential adsorption and activation of phenol on Fe, preventing its hydrogenation by palladium sites.

The deoxygenation of phenol—a key intermediate in the HDO of all lignin model molecules—on the Fe(110) and Pd(111) surfaces have been examined by McEwen and co-workers [266]. The major reaction routes identified were found to be: (i) the hydrogenation/deoxygenation mechanism, (ii) a direct deoxygenation mechanism and (iii) the tautomerization/deoxygenation mechanism. Among these, the direct C–O bond breaking was found to be the most energetically and kinetically favorable mechanism.

Cresol is another important substrate, among phenol derivatives, so far studied [267,268]. Three major reaction pathways were observed [269]: direct hydrogenolysis of Ar–OH bond (HDO), the Ar–C bond breaking (DMT) and the hydrogenation of the aromatic ring (HYD) (Figure 16).

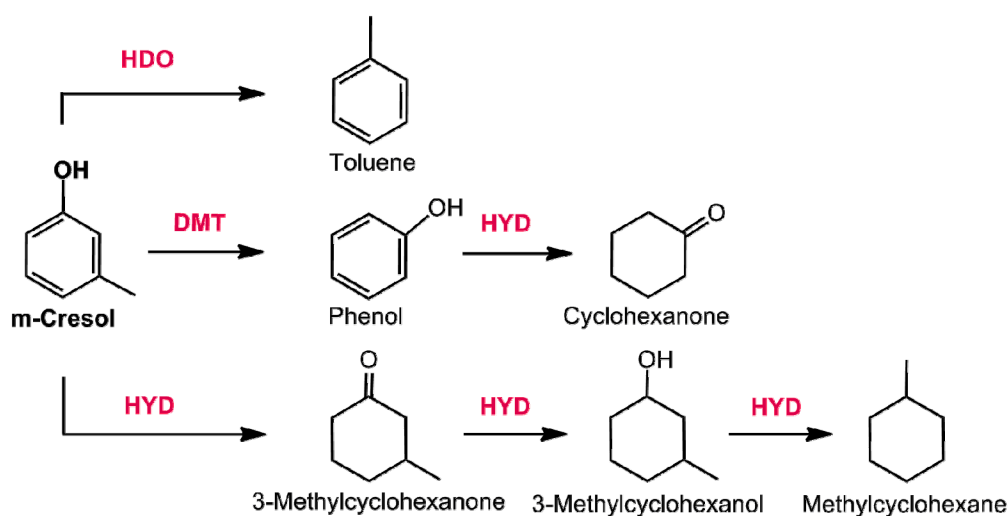


**Figure 16.** Reaction pathways observed in m-cresol HDO over Pd based catalysts (adapted from Ref. [268]).

The HDO of m-cresol was studied over a Pd-Fe catalyst as well as other Fe promoted precious metal systems [142]. Also in this case, the addition of palladium facilitates the activity of Fe in the C–O cleavage without the hydrogenation of aromatic ring. Based on DFT calculations, the role of palladium is that to stabilize the metallic Fe (catalytic site for the activation of phenolic compounds) preserving its oxidation. The lower tendency of metallic Fe to oxidize, upon of Pd addition, was also confirmed in the in situ XANES analysis. Overall, the addition of palladium influences both the adsorption of m-cresol on Fe as well as the spillover process.

Pt/Fe<sub>2</sub>O<sub>3</sub>, Ru/Fe<sub>2</sub>O<sub>3</sub> and Rh/Fe<sub>2</sub>O<sub>3</sub> samples were also investigated to understand if the synergistic effect between Pd and Fe can be extensible. The conversion of m-cresol follows the order Pd < Pt < Ru < Rh in analogy with the H<sub>2</sub> sticking probability on investigated precious metals.

### 3.2.2. Hydrogenolysis of Benzyl Phenyl Ether, 2-Phenethyl Phenyl Ether and Diphenyl Ether as Model Molecules of $\alpha$ -O-4, $\beta$ -O-4 and 4-O-5 Ether Bonds in Lignin

Various metals have been investigated as catalysts for the cleavage of the  $\alpha$ -O-4 (Benzyl Phenyl Ether—BPE),  $\beta$ -O-4 (Phenethyl Phenyl Ether—PPE) and 4-O-5 (Diphenyl Ether—DPE) lignin linkages [48–51] (Figure 17).

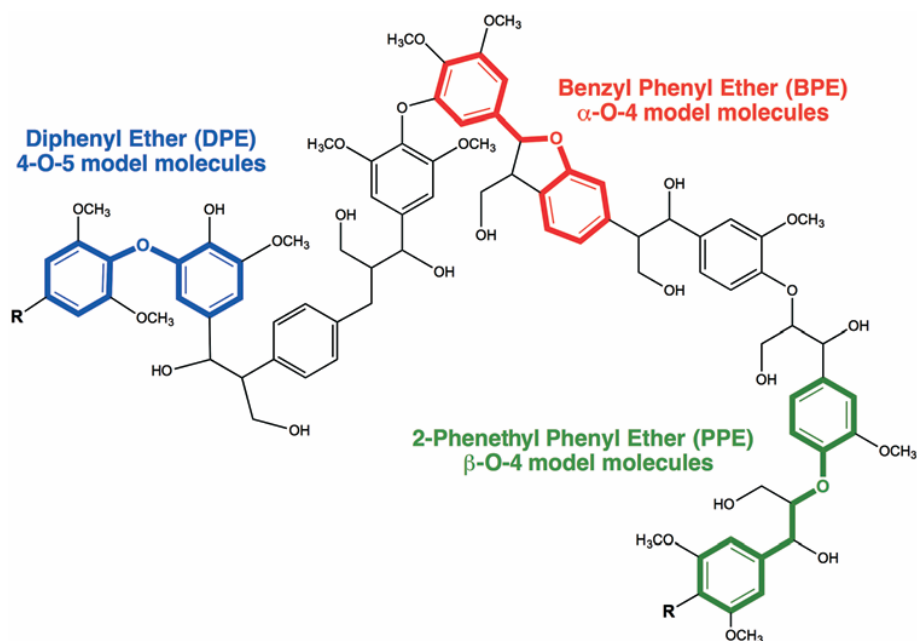


**Figure 17.** BPE, PPE and DPE as model compounds of C–O lignin linkages (Ref. [145]).

Palladium catalysts, when used, provide good results but were found to be less efficient in producing aromatic feedstocks [265]. However, one of the key objectives in the catalytic valorization of lignin is the selective cleavage of C<sub>Ar</sub>–O bond preserving its aromatic nature (aromatic ring hydrogenation consumes hydrogen and renders the reaction less useful for producing aromatics).

Benzyl phenyl ether (BPE) is the simplest model molecule representing the  $\alpha$ -O-4 ether bond of lignin and it is characterized by a weak ether bond of 218 kJ/mol [192].

The Pd-Fe/OMC catalyst was tested in the C–O bond breaking of BPE and the results were compared with those obtained with Pd/OMC and Fe/OMC samples [143] (Table 4). The aromatic yield follows the order Pd/OMC (36.2%) < Fe/OMC (37.2%) < Pd-Fe/OMC (74.3%) denoting, also in this case, the higher tendency of Pd-Fe systems in producing aromatics because of Fe addition on the Pd catalyst.

**Table 4.** Catalytic performance of heterogeneous Pd-Fe catalysts in the cleavage of C–O bond in BPE, PPE and DPE.

Catalyst	Preparation Method <sup>1</sup>	Substrate	H-Source	Temp. [°C]	Time [min]	Conversion [%]	Aromatic Yield [%]	References
Pd/OMC	STM-IWi	BPE	H <sub>2</sub> (10 bar)	250	60	93.0	36.2	[143]
Fe/OMC	STM-IWi	BPE	H <sub>2</sub> (10 bar)	250	60	50.1	37.2	[143]
Pd-Fe/OMC	STM-IWi	BPE	H <sub>2</sub> (10 bar)	250	60	88.5	74.3	[143]
Pd <sub>1</sub> -Fe <sub>0</sub> /OMC	STM-IWi	PPE	H <sub>2</sub> (10 bar)	250	180	94.1	15.1	[144]
Pd <sub>1</sub> -Fe <sub>0.25</sub> /OMC	STM-IWi	PPE	H <sub>2</sub> (10 bar)	250	180	88.3	28.3	[144]
Pd <sub>1</sub> -Fe <sub>0.7</sub> /OMC	STM-IWi	PPE	H <sub>2</sub> (10 bar)	250	180	75.6	56.7	[144]
Pd <sub>1</sub> -Fe <sub>1.5</sub> /OMC	STM-IWi	PPE	H <sub>2</sub> (10 bar)	250	180	63.2	46.6	[144]
Pd <sub>1</sub> -Fe <sub>4</sub> /OMC	STM-IWi	PPE	H <sub>2</sub> (10 bar)	250	180	41.2	31.1	[144]
Pd/Fe <sub>3</sub> O <sub>4</sub>	CP	BPE	H <sub>2</sub> (10 bar)	240	90	75.0	75.0	[145]
Pd/Fe <sub>3</sub> O <sub>4</sub>	CP	BPE	H <sub>2</sub> (20 bar)	240	90	73.0	73.0	[145]
Pd/Fe <sub>3</sub> O <sub>4</sub>	CP	BPE	H <sub>2</sub> (40 bar)	240	90	71.0	69.6	[145]
Pd/Fe <sub>3</sub> O <sub>4</sub>	CP	BPE	<i>i</i> PrOH	180	90	19.7	100	[145]
Pd/Fe <sub>3</sub> O <sub>4</sub>	CP	BPE	<i>i</i> PrOH	210	90	49.4	100	[145]
Pd/Fe <sub>3</sub> O <sub>4</sub>	CP	BPE	<i>i</i> PrOH	240	90	100	100	[145]
Pd/Fe <sub>3</sub> O <sub>4</sub>	CP	PPE	<i>i</i> PrOH	240	90	22.0	100	[145]
Pd/Fe <sub>3</sub> O <sub>4</sub>	CP	DPE	<i>i</i> PrOH	240	90	<2	-	[145]

<sup>1</sup> STM-IWi: surfactant-templating method and a subsequent incipient wetness impregnation method; CP: coprecipitation method; *i*PrOH: 2-propanol.

The same authors investigated a series of Pd-Fe catalysts with different Fe/Pd molar ratio ( $X$ ) in the hydrogenolysis of the PPE [144]. The catalytic activity was strongly influenced by the Fe/Pd molar ratio with the best results, in terms of aromatic yield, obtained with a Fe/Pd molar ratio of 0.7 (Figure 18). The hydrogen adsorption ability of the Pd-Fe catalysts was investigated by  $H_2$ -TPD. The amount of  $H_2$  desorbed found was Pd/OMC > Pd-Fe/OMC > Fe/OMC suggesting that palladium, if compared with iron, has a higher tendency to retain hydrogen [143]. Accordingly, the amount of  $H_2$  desorbed is significantly affected by the Pd/Fe molar ratio [144]. This is a crucial point that can further explain the ability of Pd-Fe systems in the C–O bond breaking in presence of the aromatic functionality.

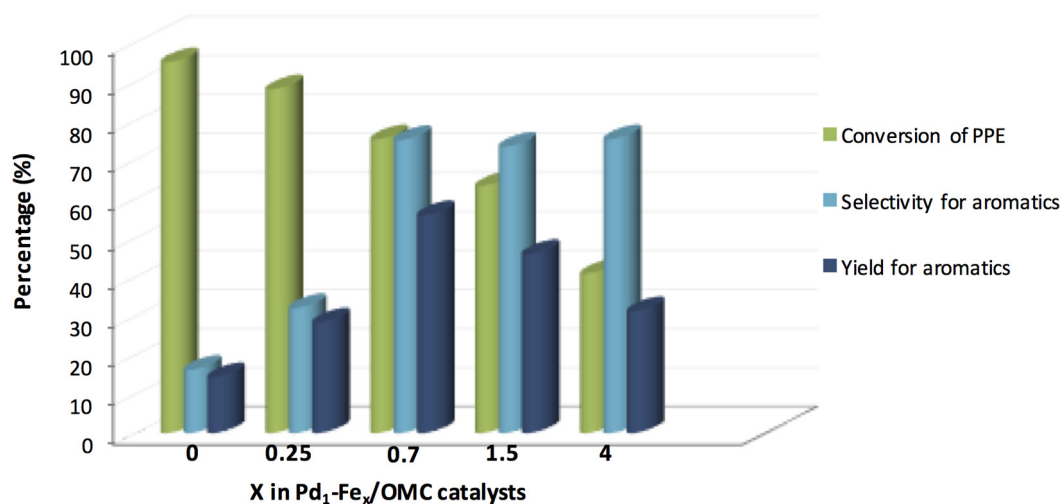


**Figure 18.** Hydrogenolysis of PPE promoted by Pd<sub>1</sub>-Fe<sub>X</sub>/OMC ( $X = 0, 0.25, 0.7, 1.5,$  and  $4$ ) catalysts (adapted from Ref. [144]).

The selective breaking of the C–O bond of BPE, PPE and DPE was recently investigated under CTH conditions [145]. On using the Pd/Fe<sub>3</sub>O<sub>4</sub> catalyst, a significant BPE (0.1 M) conversion (19.7%) was completed even at 180 °C (Table 4). The conversion grows by increasing the reaction temperature and, at 240 °C, BPE is fully converted (100% conversion) into phenol and toluene as the only reaction products (100% aromatic yield). The low tendency of the co-precipitated Pd/Fe<sub>3</sub>O<sub>4</sub> catalyst to hydrogenate the aromatic ring was previously observed [270] and confirmed with crosscheck experiments with phenol and toluene.

The C–O bond breaking of BPE was also studied under classic hydrogenolysis condition (10, 20 and 40 bar of  $H_2$ ). A decrease in BPE conversion is noticed while the selectivity to aromatics remains above 98% confirming the low tendency of the Pd/Fe<sub>3</sub>O<sub>4</sub> catalyst to hydrogenate the aromatic ring also in presence of added  $H_2$ . On the other hand, Pd/C was found to be almost inactive in the cleavage of the C–O bond under CTH conditions while, under hydrogenolysis conditions (10 bar of  $H_2$ ), a 98% of BPE conversion (40% of aromatic selectivity) was registered. The modest performance of the Pd/C catalyst in CTH reactions is related to its lower ability to dehydrogenate 2-propanol as revealed by the very small quantity of acetone formed.

The H-donor ability of simple primary and secondary alcohols was also investigated. A tight correlation between the quantity of aldehyde or ketone formed (H-donor ability) and the amount of BPE converted was found suggesting that: (i) the CTH process of BPE is very sensitive to steric hindrance of the H-donor molecule and, most important; (ii) the H-transfer from the alcohol and the hydrogen promoting the C–O bond breaking occur in a unique chemical process (Figure 19).

CTH of 2-phenethylphenylether (PPE) and diphenyl ether (DPE) was also investigated. Very interestingly, a linear correlation of the bond strength (4-O-5 = 314 kJ·mol<sup>-1</sup>; β-O-4 = 289 kJ·mol<sup>-1</sup> and α-O-4 = 218 kJ·mol<sup>-1</sup>) and the ability of the Pd/Fe<sub>3</sub>O<sub>4</sub> catalyst in the CTH of aromatic ethers was found.

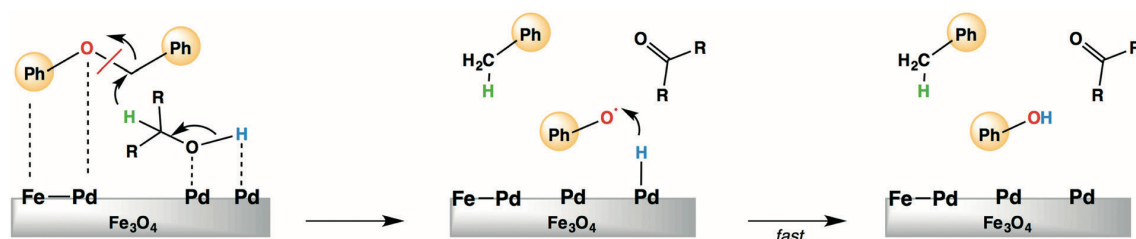


Figure 19. Pd/Fe<sub>3</sub>O<sub>4</sub>-catalyzed selective transfer hydrogenolysis of BPE (Ref. [145]).

#### 4. Conclusions and Outlook

Bimetallic Pd-Fe systems are an emerging class of heterogeneous catalysts for upgrading platform molecules deriving from lignocellulosic biomasses.

In this review, together with a detailed presentation of the various reactions promoted by Pd-Fe systems, we present the most common synthetic methods used for the preparation of different type of Pd-Fe catalysts (impregnation, deposition-precipitation and co-precipitation) as well as typical analysis techniques adopted for the physico-chemical characterization (XRD, TEM, H<sub>2</sub>-TPR, XPS and EXAFS).

The significant catalytic activity, much higher than that shown by the individual metal components, can be ascribed to the addition of Fe to palladium-based catalysts that allows the formation of Pd-Fe alloy or ensembles. X-ray photoelectron spectroscopy reveals that, in heterogeneous Pd-Fe catalysts, the Pd 3d<sub>5/2</sub> binding energy is higher than that reported for metallic palladium suggesting the presence of Pd-Fe clusters on the surface. Accordingly, EXAFS analysis discloses a shorter scattering of the Pd-Fe path than the classic Pd-Pd distance. Besides, the presence of Pd on iron oxides supports (Fe<sub>2</sub>O<sub>3</sub> and Fe<sub>3</sub>O<sub>4</sub>) enhances the reducibility of those surfaces stabilizing the reduced Fe from possible oxidation during hydrogenolysis reactions. Moreover, the electronic properties of Pd-Fe catalysts can be opportunely modified by incorporating a secondary co-metal (Zn or Co).

Hence, heterogeneous Pd-Fe catalysts may be successfully used in important sustainable reactions including the selective C-C and C-O bond cleavage of (i) C<sub>2</sub>-C<sub>6</sub> polyols; (ii) furfurals; (iii) phenol derivatives and (iv) aromatic ethers both in presence of molecular H<sub>2</sub>—as simple hydrogen source—or with indirect H<sub>2</sub> source (by dehydrogenation of alcoholic solvent or through APR of the biomass derived molecule itself).

With respect to C<sub>2</sub>-C<sub>6</sub> polyols, a preference to C-C bond breaking over that of C-O bond in the EG hydrogenolysis—strictly related with the reaction temperature—was determined over several Pd-Fe systems. Good performances of bimetallic Pd-Fe catalysts have been obtained in the preparation of 1,2-propanediol from glycerol also under CTH conditions. Furthermore, Pd-Fe systems have been demonstrated to be efficient catalysts for the renewable H<sub>2</sub> production by means of the APR process of polyols, operating under mild conditions and without formation of CO. Fe<sub>2</sub>O<sub>3</sub>-supported Pd catalysts were successfully used also in the transfer hydrogenation and hydrogenolysis of furfural derivatives as well as in the aqueous-phase hydrogenation (APH) reactions of propanal and xylose. At the same time, Pd-Fe systems are excellent catalysts for the valorization of lignin model molecules being able to cleave the C-O bond without saturation of the aromatic ring.

In view of all this, heterogeneous Pd-Fe catalysts have the potential to be successfully adopted to produce bulk and fine compounds in all the reductive processes used in modern biorefineries. While a lot of efforts have been done in their use in the hydrogenation and hydrogenolysis of platform derived molecules, a lot of research needs to be carried out to explore the use of heterogeneous Pd-Fe catalysts for the direct conversion of cellulose, hemicellulose and lignin into building block chemicals.

**Conflicts of Interest:** The authors declare no conflict of interest.

## References

1. United Nations. Adoption of the Paris Agreement. *FCCC/CP/2015/L.9/Rev.1*, 2015; pp. 1–32. Available online: <https://unfccc.int/resource/docs/2015/cop21/eng/l09r01.pdf> (accessed on 30 December 2016).
2. The White House-Washington. National Bio-economy Blueprint. 2012; pp. 1–43. Available online: [https://www.whitehouse.gov/sites/default/files/microsites/ostp/national\\_bioeconomy\\_blueprint\\_april\\_2012](https://www.whitehouse.gov/sites/default/files/microsites/ostp/national_bioeconomy_blueprint_april_2012) (accessed on 30 December 2016).
3. European Commission. Innovating for Sustainable Growth: A Bioeconomy for Europe. 2012; pp. 1–9. Available online: [http://ec.europa.eu/research/bioeconomy/pdf/official-strategy\\_en.pdf](http://ec.europa.eu/research/bioeconomy/pdf/official-strategy_en.pdf) (accessed on 30 December 2016).
4. European Commission. A Roadmap for Moving to a Competitive Low Carbon Economy in 2050. 2011. Available online: <http://eur-lex.europa.eu/legal-content/EN/ALL/?uri=CELEX:52011DC0112> (accessed on 30 December 2016).
5. European Commission. Bio-Based Economy for Europe: State of Play and Future Potential. 2011. Available online: <http://ec.europa.eu/research/bioeconomy/pdf/biobasedeconomyforeuropepart1allbrochureweb.pdf> (accessed on 30 December 2016).
6. European Commission. Horizon 2020—The Framework Programme for Research and Innovation. 2011; pp. 1–14. Available online: <http://eurlex.europa.eu/legalcontent/EN/TXT/PDF/?uri=CELEX:52011DC0808&from=EN> (accessed on 30 December 2016).
7. Lee, D.-H. Bio-based economies in Asia: Economic analysis of development of bio-based industry in China, India, Japan, Korea, Malaysia and Taiwan. *Int. J. Hydrogen Energy* **2016**, *41*, 4333–4346. [CrossRef]
8. Dey, S. Asian bioeconomy and biobusiness: Current scenario and future prospects. *New Biotechnol.* **2014**, *31*, S34. [CrossRef]
9. Tawfik, M. Asia and bioeconomy: Growing synergies. *Asian Biotechnol. Dev. Rev.* **2004**, *6*, 5–8.
10. Snyder, S.W. *Commercializing Biobased Products: Opportunities, Challenges, Benefits, and Risks*, 1st ed.; Royal Society of Chemistry: London, UK, 2015.
11. Thomopoulos, N. Global Markets for Renewable Chemicals Manufacturing. 2016; ENV032A. Available online: <http://www.bccresearch.com/market-research/environment/renewable-chemicals-manufacturing-markets-report-env032a.html> (accessed on 30 December 2016).
12. *Global Bio-Based Chemicals Market Insights, Opportunity Analysis, Market Shares and Forecast, 2016–2022*; Occams Business Research: Mumbai, India, 2016.
13. Somerville, C.; Youngs, H.; Taylor, C.; Davis, S.C.; Long, S.P. Feedstocks for lignocellulosic biofuels. *Science* **2010**, *329*, 790–792. [CrossRef] [PubMed]
14. Tuck, C.O.; Pérez, E.; Horváth, I.T.; Sheldon, R.A.; Poliakov, M. Valorization of biomass: Deriving more value from waste. *Science* **2012**, *337*, 695–699. [CrossRef] [PubMed]
15. Yan, K.; Yang, Y.; Chai, J.; Lu, Y. Catalytic reactions of gamma-valerolactone: A platform to fuels and value-added chemicals. *Appl. Catal. B Environ.* **2015**, *179*, 292–304. [CrossRef]
16. Hu, L.; Lin, L.; Wu, Z.; Zhou, S.; Liu, S. Chemocatalytic hydrolysis of cellulose into glucose over solid acid catalysts. *Appl. Catal. B Environ.* **2015**, *174–175*, 225–243. [CrossRef]
17. Negahdar, L.; Delidovich, I.; Palkovits, R. Aqueous-phase hydrolysis of cellulose and hemicelluloses over molecular acidic catalysts: Insights into the kinetics and reaction mechanism. *Appl. Catal. B Environ.* **2016**, *184*, 285–298. [CrossRef]
18. Sheldon, R.A. Green and sustainable manufacture of chemicals from biomass: State of the art. *Green Chem.* **2014**, *16*, 950–963. [CrossRef]
19. Zhang, Z.; Song, J.; Han, B. Catalytic transformation of lignocellulose into chemicals and fuel products in ionic liquids. *Chem. Rev.* **2016**. [CrossRef]
20. Li, C.; Zhao, X.; Wang, A.; Huber, G.H.; Zhang, T. Catalytic transformation of lignin for the production of chemicals and fuels. *Chem. Rev.* **2015**, *115*, 11559–11624. [CrossRef] [PubMed]
21. Lange, J.P. Lignocellulose conversion: An introduction to chemistry, process and economics. *Biofuels Bioprod. Biorefin.* **2007**, *1*, 39–48. [CrossRef]
22. Stöcker, M. Biofuels and biomass-to-liquid fuels in the biorefinery: Catalytic conversion of lignocellulosic biomass using porous materials. *Angew. Chem. Int. Ed.* **2008**, *47*, 9200–9211. [CrossRef] [PubMed]

23. Petrus, L.; Noordermeer, M.A. Biomass to biofuels, a chemical perspective. *Green Chem.* **2006**, *8*, 861–867. [[CrossRef](#)]
24. Chen, H. Chemical composition and structure of natural lignocellulose. In *Biotechnology of Lignocellulose: Theory and Practice*; Springer Science + Business Media B.V.: Dordrecht, The Netherlands, 2014; pp. 25–71.
25. Delidovich, I.; Leonhard, K.; Palkovits, R. Cellulose and hemicellulose valorisation: An integrated challenge of catalysis and reaction engineering. *Energy Environ. Sci.* **2014**, *7*, 2803–2830. [[CrossRef](#)]
26. Liu, X.; Wang, X.; Yao, S.; Jiang, Y.; Guan, J.; Mu, X. Recent advances in the production of polyols from lignocellulosic biomass and biomass-derived compounds. *RSC Adv.* **2014**, *4*, 49501–49520. [[CrossRef](#)]
27. Deng, W.; Zhang, Q.; Wang, Y. Catalytic transformation of cellulose and its derived carbohydrates into chemicals involving C–C bond cleavage. *J. Energy Chem.* **2015**, *24*, 595–607. [[CrossRef](#)]
28. Zhao, S.; Xu, G.; Chang, C.; Fang, S.; Liu, Z.; Du, F. Direct Conversion of carbohydrates into ethyl levulinate with potassium phosphotungstate as an efficient catalyst. *Catalysts* **2015**, *5*, 1897–1910. [[CrossRef](#)]
29. Antonetti, C.; Licursi, D.; Fulignati, S.; Valentini, G.; Raspolli Galletti, A.M. New frontiers in the catalytic synthesis of levulinic acid: From sugars to raw and waste biomass as starting feedstock. *Catalysts* **2016**, *6*, 196. [[CrossRef](#)]
30. Werpy, T.; Petersen, G.; Aden, A.; Bozell, J.; Holladay, J.; White, J.; Manheim, A.; Eliot, D.; Lasure, L.; Jones, S. *Top Value Added Chemicals from Biomass. Results of Screening for Potential Candidates from Sugars and Synthesis Gas*; U.S. Department of Energy: Oak Ridge, TN, USA, 2004.
31. Pagliaro, M.; Rossi, M. *The Future of Glycerol*, 2nd ed.; Royal Society of Chemistry: Cambridge, UK, 2010.
32. Zhou, C.H.; Zhao, H.; Tong, D.S.; Wu, L.M.; Yu, W.H. Recent advances in catalytic conversion of glycerol. *Catal. Rev.* **2013**, *55*, 369–453. [[CrossRef](#)]
33. Ciriminna, R.; Della Pina, C.; Rossi, M.; Pagliaro, M. Understanding the glycerol market. *Eur. J. Lipid Sci. Technol.* **2014**, *116*, 1432–1439. [[CrossRef](#)]
34. Mauriello, F.; Musolino, M.G.; Pietropaolo, R. Valorization of glycerol in propanediols production by catalytic processes: Production, structure and applications. In *Glycerol Production, Structure and Applications*; De Santos Silva, M., Ferreira, P.C., Eds.; Nova Science Publishers: New York, NY, USA, 2012; pp. 45–76.
35. Zakaria, Z.Y.; Amin, N.A.S.; Linnekoski, J. A perspective on catalytic conversion of glycerol to olefins. *Biomass Bioenergy* **2013**, *55*, 370–385. [[CrossRef](#)]
36. Tran, N.H.; Kannangara, G.S.K. Conversion of glycerol to hydrogen rich gas. *Chem. Soc. Rev.* **2013**, *42*, 9454–9479. [[CrossRef](#)] [[PubMed](#)]
37. Zhou, C.H.; Beltramini, J.N.; Fan, Y.-X.; Lu, G.Q. Chemo-selective catalytic conversion of glycerol as a biorenewable source to valuable commodity chemicals. *Chem. Soc. Rev.* **2008**, *37*, 527–549. [[CrossRef](#)] [[PubMed](#)]
38. Nakagawa, Y.; Tomishige, K. Heterogeneous catalysis of the glycerol hydrogenolysis. *Catal. Sci. Technol.* **2011**, *1*, 179–190. [[CrossRef](#)]
39. Scheller, H.V.; Ulvskov, P. Hemicelluloses. *Annu. Rev. Plant Biol.* **2010**, *61*, 263–289. [[CrossRef](#)] [[PubMed](#)]
40. Huang, Y.; Wang, L.; Chao, Y.; Nawawi, D.S.; Akiyama, T.; Yokoyama, T.; Matsumoto, Y. Relationships between hemicellulose composition and lignin structure in woods. *J. Wood Chem. Technol.* **2016**, *36*, 9–15. [[CrossRef](#)]
41. Perez, R.F.; Fraga, M.A. Hemicellulose-derived chemicals: One-step production of furfuryl alcohol from xylose. *Green Chem.* **2014**, *16*, 3942–3950. [[CrossRef](#)]
42. Carvalheiro, F.; Duarte, L.C.; Gírio, F.M. Hemicellulose biorefineries: A review on biomass pretreatment. *J. Sci. Ind. Res.* **2008**, *67*, 849–864.
43. Ji, X.-J.; Huang, H.; Nie, Z.-K.; Qu, L.; Xu, Q.; Tsao, G.T. Fuels and chemicals from hemicellulose sugars. *Adv. Biochem. Eng./Biotechnol.* **2012**, *128*, 199–224.
44. Mamman, A.S.; Lee, J.-M.; Kim, Y.-C.; Hwang, I.T.; Park, N.J.; Hwang, Y.K.; Chang, J.-S.; Hwang, J.-S. Furfural: Hemicellulose/xylose-derived biochemical. *Biofuels Bioprod. Biorefin.* **2008**, *2*, 438–454. [[CrossRef](#)]
45. Li, X.; Jia, P.; Wang, T. Furfural: A promising platform compound for sustainable production of C4 and C5 chemicals. *ACS Catal.* **2016**, *6*, 7621–7640. [[CrossRef](#)]
46. Pizzi, R.; Van Putten, R.-J.; Brust, H.; Perathoner, S.; Centi, G.; Van der Waal, J.C. High-throughput screening of heterogeneous catalysts for the conversion of furfural to bio-based fuel components. *Catalysts* **2015**, *5*, 2244–2257. [[CrossRef](#)]

47. Mariscal, R.; Maireles-Torres, P.; Ojeda, M.; Sádaba, I.; López Granados, M. Furfural: A renewable and versatile platform molecule for the synthesis of chemicals and fuels. *Energy Environ. Sci.* **2016**, *9*, 1144–1189. [[CrossRef](#)]
48. Xu, C.; Arancon, R.A.D.; Labidi, J.; Luque, R. Lignin depolymerisation strategies: Towards valuable chemicals and fuels. *Chem. Soc. Rev.* **2014**, *43*, 7485–7500. [[CrossRef](#)] [[PubMed](#)]
49. Deuss, P.J.; Barta, K. From models to lignin: Transition metal catalysis for selective bond cleavage reactions. *Coord. Chem. Rev.* **2016**, *306*, 510–532. [[CrossRef](#)]
50. Zaheer, M.; Kempe, R. Catalytic Hydrogenolysis of aryl ethers: A key step in lignin valorization to valuable chemicals. *ACS Catal.* **2015**, *5*, 1675–1684. [[CrossRef](#)]
51. Zakzeski, J.; Bruijninx, P.C.A.; Jongerius, A.L.; Weckhuysen, B.M. The catalytic valorization of lignin for the production of renewable chemicals. *Chem. Rev.* **2010**, *110*, 3552–3599. [[CrossRef](#)] [[PubMed](#)]
52. Robinson, A.M.; Hensley, J.E.; Medlin, J.W. Bifunctional catalysts for upgrading of biomass-derived oxygenates: A review. *ACS Catal.* **2016**, *6*, 5026–5043. [[CrossRef](#)]
53. Sergeev, A.G.; Hartwig, J.F. Selective, nickel-catalyzed hydrogenolysis of aryl ethers. *Science* **2011**, *332*, 439–443. [[CrossRef](#)] [[PubMed](#)]
54. Sergeev, A.G.; Webb, J.D.; Hartwig, J.F. A heterogeneous nickel catalyst for the hydrogenolysis of aryl ethers without arene hydrogenation. *J. Am. Chem. Soc.* **2012**, *134*, 20226–20229. [[CrossRef](#)] [[PubMed](#)]
55. He, J.; Zhao, C.; Lercher, J.A. Ni-catalyzed cleavage of aryl ethers in the aqueous phase. *J. Am. Chem. Soc.* **2012**, *134*, 20768–20775. [[CrossRef](#)] [[PubMed](#)]
56. He, J.; Lu, L.; Zhao, C.; Mei, D.; Lercher, J.A. Mechanisms of catalytic cleavage of benzyl phenyl ether in aqueous and apolar phases. *J. Catal.* **2014**, *311*, 41–51. [[CrossRef](#)]
57. He, J.; Lu, L.; Zhao, C.; Mei, D.; Lercher, J.A. Mechanisms of selective cleavage of C–O bonds in diaryl ethers in aqueous phase. *J. Catal.* **2014**, *309*, 280–290. [[CrossRef](#)]
58. Wang, X.; Rinaldi, R. A route for lignin and bio-oil conversion: Dehydroxylation of phenols into arenes by catalytic tandem reactions. *Angew. Chem. Int. Ed.* **2013**, *52*, 11499–11503. [[CrossRef](#)] [[PubMed](#)]
59. Wang, X.; Rinaldi, R. Solvent effects on the hydrogenolysis of diphenyl ether with raney nickel and their implications for the conversion of lignin. *ChemSusChem* **2012**, *5*, 1455–1466. [[CrossRef](#)] [[PubMed](#)]
60. Macala, G.S.; Matson, T.D.; Johnson, C.L.; Lewis, R.S.; Iretskii, A.V.; Ford, P.C. Hydrogen transfer from supercritical methanol over a solid base catalyst: A model for lignin depolymerization. *ChemSusChem* **2009**, *2*, 215–217. [[CrossRef](#)] [[PubMed](#)]
61. Barta, K.; Matson, T.D.; Fettig, M.L.; Scott, S.L.; Iretskii, A.V.; Ford, P.C. Catalytic disassembly of an organosolv lignin via hydrogen transfer from supercritical methanol. *Green Chem.* **2010**, *12*, 1640–1648. [[CrossRef](#)]
62. Galkin, M.V.; Sawadjoon, S.; Rohde, V.; Dawange, M.; Samec, J.S.M. Mild Heterogeneous Palladium-catalyzed cleavage of  $\beta$ -O-4'-ether linkages of lignin model compounds and native lignin in air. *ChemCatChem* **2013**, *6*, 179–184. [[CrossRef](#)]
63. Galkin, M.V.; Samec, J.S.M. Selective route to 2-propenyl aryls directly from wood by a tandem organosolv and palladium-catalysed transfer hydrogenolysis. *ChemSusChem* **2014**, *7*, 2154–2158. [[CrossRef](#)] [[PubMed](#)]
64. Galkin, M.V.; Dahlstrand, C.; Samec, J. Mild and robust redox-neutral Pd/C-catalyzed lignol  $\beta$ -O-4' bond cleavage through a low-energy-barrier pathway. *ChemSusChem* **2015**, *8*, 2187–2192. [[CrossRef](#)] [[PubMed](#)]
65. Toledano, A.; Serrano, L.; Labidi, J.; Pineda, A.; Balu, A.M.; Luque, R. Heterogeneously catalysed mild hydrogenolytic depolymerisation of lignin under microwave irradiation with hydrogen-donating solvents. *ChemCatChem* **2012**, *5*, 977–985. [[CrossRef](#)]
66. De, S.; Saha, B.; Luque, R. Hydrodeoxygenation processes: Advances on catalytic transformations of biomass-derived platform chemicals into hydrocarbon fuels. *Bioresour. Technol.* **2015**, *178*, 108–118. [[CrossRef](#)] [[PubMed](#)]
67. Dawes, G.J.S.; Scott, E.L.; Le Nôtre, J.; Sanders, J.P.M.; Bitter, J.H. Deoxygenation of biobased molecules by decarboxylation and decarbonylation—A review on the role of heterogeneous, homogeneous and bio-catalysis. *Green Chem.* **2015**, *17*, 3231. [[CrossRef](#)]
68. Ruppert, A.M.; Weinberg, K.; Palkovits, R. Hydrogenolysis goes bio: From carbohydrates and sugar alcohols to platform chemicals. *Angew. Chem. Int. Ed.* **2012**, *51*, 2564–2601. [[CrossRef](#)] [[PubMed](#)]
69. Wang, D.; Astruc, D. The golden age of transfer hydrogenation. *Chem. Rev.* **2015**, *115*, 6621–6686. [[CrossRef](#)] [[PubMed](#)]

70. Johnstone, R.A.W.; Wilby, A.H.; Entwistle, I.D. Heterogeneous catalytic transfer hydrogenation and its relation to other methods for reduction of organic compounds. *Chem. Rev.* **1985**, *85*, 129–170. [CrossRef]
71. Brieger, G.; Nestrick, T.J. Catalytic transfer hydrogenation. *Chem. Rev.* **1974**, *74*, 567–580. [CrossRef]
72. Gilkey, M.J.; Xu, B. Heterogeneous catalytic transfer hydrogenation as an effective pathway in biomass upgrading. *ACS Catal.* **2016**, *6*, 1420–1436. [CrossRef]
73. Knoevenagel, E.; Bergdolt, B. Ueber das Verhalten des  $\Delta_{2,5}$ -Dihydroterephthalsäuredimethylesters bei höheren Temperaturen und in Gegenwart von Palladiummohr. *Eur. J. Inorg. Chem.* **1903**, *36*, 2857–2860. [CrossRef]
74. Cortright, R.D.; Davda, R.R.; Dumesic, J.A. Hydrogen from catalytic reforming of biomass-derived hydrocarbons in liquid water. *Nature* **2002**, *418*, 964–967. [CrossRef]
75. Davda, R.R.; Dumesic, J.A. Catalytic reforming of oxygenated hydrocarbons for hydrogen with low levels of carbon monoxide. *Angew. Chem. Int. Ed.* **2003**, *42*, 4068–4071. [CrossRef] [PubMed]
76. Metzger, J.O. Production of liquid hydrocarbons from biomass. *Angew. Chem. Int. Ed.* **2006**, *45*, 696–698. [CrossRef] [PubMed]
77. Kunkes, E.L.; Simonetti, D.A.; West, R.M.; Serrano-Ruiz, J.C.; Gärtner, C.A.; Dumesic, J.A. Catalytic conversion of biomass to monofunctional hydrocarbons and targeted liquid-fuel classes. *Science* **2008**, *322*, 417–421. [CrossRef] [PubMed]
78. Davda, R.R.; Shabaker, J.W.; Huber, G.W.; Cortright, R.D.; Dumesic, J.A. Aqueous-phase reforming of ethylene glycol on silica-supported metal catalysts. *Appl. Catal. B Environ.* **2003**, *43*, 13–26. [CrossRef]
79. Davda, R.R.; Shabaker, J.W.; Huber, G.W.; Cortright, R.D.; Dumesic, J.A. A review of catalytic issues and process conditions for renewable hydrogen and alkanes by aqueous-phase reforming of oxygenated hydrocarbons over supported metal catalysts. *Appl. Catal. B Environ.* **2005**, *56*, 171–186. [CrossRef]
80. Huber, G.W.; Shabaker, J.W.; Dumesic, J.A. Raney Ni-Sn catalyst for H<sub>2</sub> production from biomass-derived hydrocarbons. *Science* **2003**, *300*, 2075–2077. [CrossRef] [PubMed]
81. Shabaker, J.W.; Davda, R.R.; Huber, G.W.; Cortright, R.D.; Dumesic, J.A. Aqueous-phase reforming of methanol and ethylene glycol over alumina-supported platinum catalysts. *J. Catal.* **2003**, *215*, 344–352. [CrossRef]
82. Shabaker, J.W.; Dumesic, J.A. Kinetics of aqueous-phase reforming of oxygenated hydrocarbons: Pt/Al<sub>2</sub>O<sub>3</sub> and Sn-modified Ni catalysts. *Ind. Eng. Chem. Res.* **2004**, *43*, 3105–3112. [CrossRef]
83. Shabaker, J.W.; Huber, G.W.; Davda, R.R.; Cortright, R.D.; Dumesic, J.A. Aqueous-phase reforming of ethylene glycol over supported platinum catalysts. *Catal. Lett.* **2003**, *88*, 1–8. [CrossRef]
84. Shabaker, J.W.; Huber, G.W.; Dumesic, J.A. Aqueous-phase reforming of oxygenated hydrocarbons over Sn-modified Ni catalysts. *J. Catal.* **2004**, *222*, 180–191. [CrossRef]
85. Shabaker, J.W.; Simonetti, D.A.; Cortright, R.D.; Dumesic, J.A. Sn-modified Ni catalysts for aqueous-phase reforming: Characterization and deactivation studies. *J. Catal.* **2005**, *231*, 67–76. [CrossRef]
86. Frusteri, F.; Italiano, G.; Espro, C.; Arena, F.; Parmaliana, A. Doped Ni thin layer catalysts for catalytic decomposition of natural gas to produce hydrogen. *Appl. Catal. A Gen.* **2009**, *365*, 122–129.
87. Frusteri, F.; Italiano, G.; Espro, C.; Cannilla, C.; Bonura, G. H<sub>2</sub> Production by methane decomposition: Catalytic and technological aspects. *Int. J. Hydrogen Energy* **2012**, *37*, 16367–16374. [CrossRef]
88. Kettler, P.B. Platinum group metals in catalysis: Fabrication of catalysts and catalyst precursors. *Org. Proc. Res. Dev.* **2003**, *7*, 342–354. [CrossRef]
89. Wells, P.B.; Wilkinson, A.G. Platinum group metals as heterogeneous enantioselective catalysts. *Top. Catal.* **1998**, *5*, 39–50. [CrossRef]
90. Acres, G.J.K. Platinum group metal catalysis at the end of this century. *Platinum Met. Rev.* **1984**, *28*, 150–157. [CrossRef]
91. Hartley, F. *Chemistry of the Platinum Group Metals*, 1st ed.; Elsevier Science: Central Milton Keynes, UK, 2008.
92. Heraeus, Platinum & Palladium Focus 2016. Available online: [https://www.heraeus.com/media/media/group/doc\\_group/precious\\_metals/Platinum\\_Palladium\\_Focus\\_2016Europe.pdf](https://www.heraeus.com/media/media/group/doc_group/precious_metals/Platinum_Palladium_Focus_2016Europe.pdf) (accessed on 30 December 2016).
93. ETF Securities (US) LLC. Platinum and Palladium: Riding the Wave of an Expanding Auto Market. Available online: <https://www.etfsecurities.com/Documents/PP%20Commentary%20submitted%20to%20ALPS.pdf> (accessed on 30 December 2016).
94. Tungler, A.; Tarnai, T.; Hegediis, L.; Fodor, K. Palladium-mediated heterogeneous catalytic hydrogenations. *Platinum Met. Rev.* **1998**, *42*, 108–115.

95. Astruc, D.; Lu, F.; Aranzaes, J.R. Nanoparticles as recyclable catalysts: The frontier between homogeneous and heterogeneous catalysis. *Angew. Chem. Int. Ed.* **2005**, *48*, 7852–7872. [[CrossRef](#)] [[PubMed](#)]
96. Brennfürher, A.; Neumann, H.; Beller, M. Palladium-catalyzed carbonylation reactions of aryl halides and related compounds. *Angew. Chem. Int. Ed.* **2009**, *48*, 4114–4133. [[CrossRef](#)] [[PubMed](#)]
97. Yin, L.; Liebscher, J. Carbon-carbon coupling reactions catalyzed by heterogeneous palladium catalysts. *Chem. Rev.* **2007**, *107*, 133–173. [[CrossRef](#)] [[PubMed](#)]
98. Blaser, H.-U.; Malan, C.; Pugin, B.; Spindler, F.; Steiner, H.; Studer, M. Selective hydrogenation for fine chemicals: Recent trends and new developments. *Adv. Synth. Catal.* **2003**, *346*, 103–151. [[CrossRef](#)]
99. Grigg, R.; Mutton, S.P. Pd-catalysed carbonylations: Versatile technology for discovery and process chemists. *Tetrahedron* **2010**, *66*, 5515–5548. [[CrossRef](#)]
100. Genet, J.P.; Savignac, M. Recent developments of palladium (0) catalyzed reactions in aqueous medium. *J. Organomet. Chem.* **1999**, *576*, 305–317. [[CrossRef](#)]
101. Chen, X.; Engle, K.M.; Wang, D.-H.; Jin-Quan, Y. Palladium(II)-catalyzed C–H activation/C–C cross-coupling reactions: Versatility and practicality. *Angew. Chem. Int. Ed.* **2009**, *48*, 5094–5115. [[CrossRef](#)] [[PubMed](#)]
102. Beccalli, E.M.; Broggini, G.; Martinelli, M.; Sottocornola, S. C–C, C–O, C–N bond formation on sp<sup>2</sup> carbon by Pd(II)-catalyzed reactions involving oxidant agents. *Chem. Rev.* **2007**, *107*, 5318–5365. [[CrossRef](#)] [[PubMed](#)]
103. Astruc, D. Palladium nanoparticles as efficient green homogeneous and heterogeneous carbon-carbon coupling precatalysts: A unifying view. *Inorg. Chem.* **2007**, *46*, 1884–1894. [[CrossRef](#)] [[PubMed](#)]
104. Antolini, E. Palladium in fuel cell catalysis. *Energy Environ. Sci.* **2009**, *2*, 915–931. [[CrossRef](#)]
105. Kiviaho, J.; Hanaoka, T.; Kubota, Y.; Sugi, Y. Heterogeneous palladium catalysts for the Heck reaction. *J. Mol. Catal. A Chem.* **1995**, *101*, 25–31. [[CrossRef](#)]
106. Pagliaro, M.; Pandarus, V.; Ciriminna, R.; Béland, F.; Carà, P.D. Heterogeneous versus homogeneous palladium catalysts for cross-coupling reactions. *ChemCatChem* **2012**, *4*, 432–445. [[CrossRef](#)]
107. Hartings, M. Reactions coupled to palladium. *Nat. Chem.* **2012**, *4*, 764. [[CrossRef](#)] [[PubMed](#)]
108. Liao, F.; Lo, T.W.B.; Tsang, S.C.E. Recent developments in palladium-based bimetallic catalysts. *ChemCatChem* **2015**, *7*, 1998–2014. [[CrossRef](#)]
109. Coq, B.; Figueras, F. Bimetallic palladium catalysts: Influence of the co-metal on the catalyst performance. *J. Mol. Catal. A Chem.* **2001**, *173*, 117–134. [[CrossRef](#)]
110. Bond, G.C. Metal-support and metal-additive effects in catalysis. *Platinum Met. Rev.* **1983**, *21*, 16–18.
111. Banadaki, A.D.; Kajbafvala, A. Recent advances in facile synthesis of bimetallic nanostructures: An overview. *J. Nanomater.* **2014**, *2014*, 985948.
112. De, S.; Zhang, J.; Luque, R.; Yan, N. Ni-based bimetallic heterogeneous catalysts for energy and environmental applications. *Energy Environ. Sci.* **2016**, *9*, 3314–3347. [[CrossRef](#)]
113. Sankar, M.; Dimitratos, N.; Miedziak, P.J.; Wells, P.P.; Kiely, C.J.; Hutchings, G.J. Designing bimetallic catalysts for a green and sustainable future. *Chem. Soc. Rev.* **2012**, *41*, 8099–8139. [[CrossRef](#)] [[PubMed](#)]
114. Alonso, D.M.; Wettstein, S.G.; Dumesic, J.A. Bimetallic catalysts for upgrading of biomass to fuels and chemicals. *Chem. Soc. Rev.* **2012**, *41*, 8075–8098. [[CrossRef](#)] [[PubMed](#)]
115. Gao, F.; Goodman, D.W. Pd–Au bimetallic catalysts: Understanding alloy effects from planar models and (supported) nanoparticles. *Chem. Soc. Rev.* **2012**, *41*, 8009–8020. [[CrossRef](#)] [[PubMed](#)]
116. Conant, T.; Karim, A.M.; Lebarbier, V.; Wang, Y.; Girgsdies, F.; Schlögl, R.; Datye, A. Stability of bimetallic Pd–Zn catalysts for the steam reforming of methanol. *J. Catal.* **2008**, *257*, 64–70. [[CrossRef](#)]
117. Sarkany, A.; Zsoldos, Z.; Stefler, G.; Hightower, J.W.; Gucci, L. Promoter effect of Pd in hydrogenation of 1,3-butadiene over Co–Pd catalysts. *J. Catal.* **1995**, *157*, 179–189. [[CrossRef](#)]
118. Menezes, W.G.; Altmann, L.; Zielasek, V.; Thiel, K.; Bäumer, M. Bimetallic Co–Pd catalysts: Study of preparation methods and their influence on the selective hydrogenation of acetylene. *J. Catal.* **2013**, *300*, 125–135. [[CrossRef](#)]
119. Zhang, R.; Shuai, D.; Guy, K.A.; Shapley, J.R.; Strathmann, T.J.; Werth, C.J. Elucidation of Nitrate Reduction Mechanisms on a Pd–In Bimetallic Catalyst using Isotope Labeled Nitrogen Species. *ChemCatChem* **2013**, *5*, 313–321. [[CrossRef](#)]
120. Yin, Z.; Zhou, W.; Gao, Y.; Ma, D.; Kiely, C.J.; Bao, X. Supported Pd–Cu bimetallic nanoparticles that have high activity for the electrochemical oxidation of methanol. *Chem.-Eur. J.* **2012**, *18*, 4887–4893. [[CrossRef](#)] [[PubMed](#)]

121. Alshammari, V.A.; Kalevaru, N.; Martin, A. Bimetallic catalysts containing gold and palladium for environmentally important reactions. *Catalysts* **2016**, *6*, 97. [[CrossRef](#)]
122. Iwasa, N.; Masuda, S.; Ogawa, N.; Takezawa, N. Steam reforming of methanol over Pd/ZnO: Effect of the formation of PdZn alloys upon the reaction. *Appl. Catal. A Gen.* **1995**, *125*, 145–157. [[CrossRef](#)]
123. Liao, F.; Lo, B.T.; Sexton, D.; Qu, J.; Ma, C.; Chan, R.C.-T.; Lu, Q.; Che, R.; Kwok, W.-M.; He, H.; et al. A new class of tunable hetero-junction by using two support materials for the synthesis of supported bimetallic catalysts. *ChemCatChem* **2015**, *7*, 230–235. [[CrossRef](#)]
124. Tao, F.; Grass, M.E.; Zhang, Y.; Butcher, D.R.; Renzas, J.R.; Liu, Z.; Chung, J.Y.; Mun, B.S.; Salmeron, M.; Somorjai, G.A. Reaction-driven restructuring of Rh-Pd and Pt-Pd core-shell nanoparticles. *Science* **2008**, *322*, 932–934. [[CrossRef](#)] [[PubMed](#)]
125. Scott, R.W.J.; Wilson, O.M.; Oh, S.-K.; Kenik, E.A.; Crooks, R.M. Bimetallic Palladium–Gold dendrimer-encapsulated catalysts. *J. Am. Chem. Soc.* **2004**, *126*, 15583–15591. [[CrossRef](#)] [[PubMed](#)]
126. Peng, Z.; Yang, H. Synthesis and Oxygen reduction electrocatalytic property of Pt-on-Pd bimetallic hetero-nanostructures. *J. Am. Chem. Soc.* **2009**, *131*, 7542–7543. [[CrossRef](#)] [[PubMed](#)]
127. Raja, R.; Hermans, S.; Shephard, D.S.; Johnson, B.F.G.; Raja, R.; Sankar, G.; Bromley, S.; Thomas, J.M. Preparation and characterization of a highly active bimetallic (Pd–Ru) nanoparticle heterogeneous catalyst. *Chem. Commun.* **1999**, *16*, 1571–1572. [[CrossRef](#)]
128. Liu, J.; Sun, B.; Hu, J.; Pei, Y.; Li, H.; Qiao, M. Aqueous-phase reforming of ethylene glycol to hydrogen on Pd/Fe<sub>3</sub>O<sub>4</sub> catalyst prepared by co-precipitation: Metal–support interaction and excellent intrinsic activity. *J. Catal.* **2010**, *274*, 287–295. [[CrossRef](#)]
129. Mauriello, F.; Vinci, A.; Espro, C.; Gumina, B.; Musolino, M.G.; Pietropaolo, R. Hydrogenolysis vs. aqueous phase reforming (APR) of glycerol promoted by a heterogeneous Pd/Fe catalyst. *Catal. Sci. Technol.* **2015**, *5*, 4466–4473. [[CrossRef](#)]
130. Huber, G.W.; Shabaker, J.W.; Evans, S.T.; Dumesic, J.A. Aqueous-phase reforming of ethylene glycol over supported Pt and Pd bimetallic catalysts. *Appl. Catal. B Environ.* **2006**, *62*, 226–236. [[CrossRef](#)]
131. Wu, C.T.; Yu, K.M.K.; Liao, F.; Young, N.; Nellist, P.; Dent, A.; Kroner, A.; Tsang, S.C.E. A non-syn-gas catalytic route to methanol production. *Nat. Commun.* **2012**, *3*, 1050. [[CrossRef](#)] [[PubMed](#)]
132. Liao, F.; Lo, T.W.B.; Sexton, D.; Qu, J.; Wu, C.-T.; Tsang, S.C.E. PdFe nanoparticles as selective catalysts for C–C cleavage in hydrogenolysis of vicinal diol units in biomass-derived chemicals. *Catal. Sci. Technol.* **2015**, *5*, 887–896. [[CrossRef](#)]
133. Liao, F.; Lo, T.W.B.; Qu, J.; Wu, K.A.; Dent, A.; Tsang, S.C.E. Tunability of catalytic properties of Pd-based catalysts by rational control of strong metal and support interaction (SMSI) for selective hydrogenolytic C–C and C–O bond cleavage of ethylene glycol units in biomass molecules. *Catal. Sci. Technol.* **2015**, *7*, 3491–3495. [[CrossRef](#)]
134. Ge, J.; Zeng, Z.; Liao, F.; Zheng, W.; Hong, Z.; Tsang, S.C.E. Palladium on iron oxide nanoparticles: The morphological effect of the support in glycerol hydrogenolysis. *Green Chem.* **2013**, *15*, 2064–2069. [[CrossRef](#)]
135. Musolino, M.G.; Scarpino, L.A.; Mauriello, F.; Pietropaolo, R. Glycerol hydrogenolysis promoted by supported Palladium catalysts. *ChemSusChem* **2011**, *4*, 1143–1150. [[CrossRef](#)] [[PubMed](#)]
136. Jiang, T.; Huai, Q.; Geng, T.; Ying, W.; Xiao, T.; Cao, F. Catalytic performance of PdNi bimetallic catalyst for glycerol hydrogenolysis biomass and bioenergy. *Biomass Bioenergy* **2015**, *78*, 71–79. [[CrossRef](#)]
137. Musolino, M.G.; Scarpino, L.A.; Mauriello, F.; Pietropaolo, R. Selective transfer hydrogenolysis of glycerol promoted by palladium catalysts in absence of hydrogen. *Green Chem.* **2009**, *11*, 1511–1513. [[CrossRef](#)]
138. Mauriello, F.; Ariga, H.; Musolino, M.G.; Pietropaolo, R.; Takakusagi, S.; Asakura, K. Exploring the catalytic properties of supported palladium catalysts in the transfer hydrogenolysis of glycerol. *Appl. Catal. B Environ.* **2015**, *166–167*, 121–131. [[CrossRef](#)]
139. Scholz, D.; Aellig, C.; Hermans, I. Catalytic transfer hydrogenation/hydrogenolysis for reductive upgrading of furfural and 5-(hydroxymethyl) furfural. *ChemSusChem* **2014**, *7*, 268–275. [[CrossRef](#)] [[PubMed](#)]
140. Lee, J.; Kim, Y.T.; Huber, G.W. Aqueous-phase hydrogenation and hydrodeoxygenation of biomass-derived oxygenates with bimetallic catalysts. *Green Chem.* **2014**, *16*, 708–718. [[CrossRef](#)]
141. Sun, J.; Karim, A.M.; Zhang, H.; Kovarik, L.; Li, X.S.; Hensley, A.J.; McEwen, J.-S.; Wang, Y. Carbon-supported bimetallic Pd-Fe catalysts for vapor-phase hydrodeoxygenation of guaiacol. *J. Catal.* **2013**, *306*, 47–57. [[CrossRef](#)]

142. Hong, Y.; Zhang, H.; Sun, J.; Ayman, K.M.; Hensley, A.J.R.; Gu, M.; Engelhard, M.H.; McEwen, J.-S.; Wang, Y. Synergistic catalysis between Pd and Fe in gas phase hydrodeoxygenation of m-cresol. *ACS Catal.* **2014**, *4*, 3335–3345. [[CrossRef](#)]
143. Kim, J.K.; Lee, J.K.; Kang, K.H.; Song, J.C.; Song, I.K. Selective cleavage of C–O bond in benzyl phenyl ether to aromatics over Pd-Fe bimetallic catalyst supported on ordered mesoporous carbon. *Appl. Catal. A Gen.* **2015**, *498*, 142–149. [[CrossRef](#)]
144. Kim, J.K.; Lee, J.K.; Kang, K.H.; Lee, J.W.; Song, I.K. Catalytic decomposition of phenethyl phenyl ether to aromatics over Pd-Fe bimetallic catalysts supported on ordered mesoporous carbon. *J. Mol. Catal. A Chem.* **2015**, *410*, 184–192. [[CrossRef](#)]
145. Paone, E.; Espro, C.; Pietropaolo, R.; Mauriello, F. Selective arene production from transfer hydrogenolysis of benzyl phenyl ether promoted by a co-precipitated Pd/Fe<sub>3</sub>O<sub>4</sub> catalyst. *Catal. Sci. Technol.* **2016**, *6*, 7937–7941. [[CrossRef](#)]
146. Guzzi, L. Bimetallic nano-particles: Featuring structure and reactivity. *Catal. Today* **2005**, *101*, 53–64. [[CrossRef](#)]
147. Guzzi, L. Structure and promotion of bimetallic catalysts: Activity and selectivity. *Catal. Lett.* **1990**, *7*, 205–212. [[CrossRef](#)]
148. Coq, B.; Hub, S.; Figuéras, F.; Tournigant, D. Conversion under hydrogen of dichlorodifluoromethane over bimetallic palladium catalysts. *Appl. Catal. A Gen.* **1993**, *101*, 41–50. [[CrossRef](#)]
149. Lebedeva, O.E.; Chiou, W.A.; Sachtler, W.M.H. Chloride induced migration of supported platinum and palladium across phase boundaries. *Catal. Lett.* **2000**, *66*, 189–195. [[CrossRef](#)]
150. Li, W.; Halder, P. Supportless PdFe nanorods as highly active electrocatalyst for proton exchange membrane fuel cell. *Electrochem. Commun.* **2009**, *11*, 1195–1198. [[CrossRef](#)]
151. Ghauch, A.; Abou Assi, H.; Bdeir, S. Aqueous removal of diclofenac by plated elemental iron: Bimetallic systems. *J. Hazard. Mater.* **2010**, *182*, 64–74. [[CrossRef](#)] [[PubMed](#)]
152. Zhang, Z.; More, K.L.; Sun, K.; Wu, Z.; Li, W. Preparation and characterization of PdFe nanoleaves as electrocatalysts for oxygen reduction reaction. *Chem. Mater.* **2011**, *23*, 1570–1577. [[CrossRef](#)]
153. Wang, H.F.; Kaden, W.E.; Dowler, R.; Sterrer, M.; Freund, H.J. Model oxide supported metal catalysts Comparison of ultrahigh vacuum and solution based preparation of Pd nanoparticles on a single crystalline oxide substrate. *Phys. Chem. Chem. Phys.* **2012**, *14*, 11525–11533. [[CrossRef](#)] [[PubMed](#)]
154. Zhang, Z.; Zhang, C.; Sun, J.; Kou, T.; Bai, Q.; Wang, Y.; Ding, Y. Ultrafine nanoporous PdFe/Fe<sub>3</sub>O<sub>4</sub> catalysts with doubly enhanced activities towards electro oxidation of methanol and ethanol in alkaline media. *J. Mater. Chem. A* **2013**, *1*, 3620–3628. [[CrossRef](#)]
155. Han, B.; Xu, C. Nanoporous PdFe alloy as highly active and durable electrocatalyst for oxygen reduction reaction. *Int. J. Hydrogen En.* **2014**, *39*, 18247–18255. [[CrossRef](#)]
156. Wang, J.; Wang, Z.; Zhao, D.; Xu, C. Facile fabrication of nanoporous PdFe alloy for nonenzymatic electrochemical sensing of hydrogen peroxide and glucose. *Anal. Chim. Acta* **2014**, *832*, 34–43. [[CrossRef](#)] [[PubMed](#)]
157. Wang, J.; Zhou, H.; Fan, D.; Zhao, D.; Xu, C. A glassy carbon electrode modified with nanoporous PdFe alloy for highly sensitive continuous determination of nitrite. *Microchim. Acta* **2015**, *182*, 1055–1061. [[CrossRef](#)]
158. Kang, Y.S.; Choi, K.H.; Ahn, D.; Lee, M.J.; Baik, J.; Chung, D.Y.; Kim, M.J.; Lee, S.Y.; Kim, M.; Shin, H.; et al. Effect of post heat-treatment of composition controlled PdFe nanoparticles for oxygen reduction reaction. *J. Power Sources* **2016**, *303*, 234–242. [[CrossRef](#)]
159. Zhou, Y.; Du, C.; Han, G.; Gao, Y.; Yin, G. Ultralow Pt decorated PdFe Alloy Nanoparticles for Formic Acid Electro oxidation. *Electrochim. Acta* **2016**, *217*, 203–209. [[CrossRef](#)]
160. Leng, L.; Li, J.; Zeng, X.; Song, H.; Shu, T.; Wang, H.; Liao, S. Enhancing the cyclability of Li–O<sub>2</sub> batteries using PdM alloy nanoparticles anchored on nitrogen doped reduced graphene as the cathode catalyst. *J. Power Sources* **2017**, *337*, 173–179. [[CrossRef](#)]
161. Lieltz, G.; Nimz, M.; Völter, J.; Lázár, K.; Guzzi, L. Double promotion of palladium/silica catalysts by iron and magnesium oxide in the synthesis of methanol from carbon monoxide and hydrogen. *Appl. Catal.* **1988**, *45*, 71–83. [[CrossRef](#)]
162. Fukuoka, A.; Kimura, T.; Ichikawa, M. Selective Hydrogenation of CO into C1 and C2 Alcohols by SiO<sub>2</sub>-supported RhFe, PtFe, and PdFe Bimetallic Cluster-derived Catalysts. *J. Chem. Soc. Commun.* **1988**, 428–430. [[CrossRef](#)]

163. Lázár, K.; Nimz, M.; Lietz, G.; Völter, J.; Guczi, L. Formation of PdFe alloys on silica supported catalysts. *Hyperfine Interact.* **1988**, *41*, 657–660. [[CrossRef](#)]
164. Felicissimo, M.P.; Martyanov, O.N.; Risse, T.; Freund, H.-J. Characterization of a Pd-Fe bimetallic model catalyst. *Surf. Sci.* **2007**, *601*, 2105–2116. [[CrossRef](#)]
165. Fukuoka, A.; Kimura, T.; Rao, L.F.; Ichikawa, M. Heteronuclear CO activation in CO based reactions catalyzed by SiO<sub>2</sub> supported RhFe and PdFe bimetallic clusters. *Catal. Today* **1989**, *6*, 55–62. [[CrossRef](#)]
166. Fukuoka, A.; Kimura, T.; Kosugi, N.; Kuroda, H.; Minai, Y.; Sakai, Y.; Tominaga, T.; Ichikawa, M. Bimetallic promotion of alcohol production in CO hydrogenation and olefin hydroformylation on RhFe, PtFe, PdFe, and IrFe cluster derived catalysts. *J. Catal.* **1990**, *126*, 434–450. [[CrossRef](#)]
167. Pinna, F.; Selva, M.; Signoretto, M.; Strukul, G.; Boccuzzi, F.; Benedetti, A.; Canton, P.; Fagherazzi, G. Pd-Fe/SiO<sub>2</sub> Catalysts in the hydrogenation of 2,4-Dinitrotoluene. *J. Catal.* **1994**, *150*, 356–367. [[CrossRef](#)]
168. Komatsu, T.; Inaba, K.; Uezono, T.; Onda, A.; Yashima, T. Nanosize particles of palladium intermetallic compounds as catalysts for oxidative acetoxylation. *Appl. Catal. A Gen.* **2003**, *251*, 315–326. [[CrossRef](#)]
169. Garten, R.L.; Ollis, D.F. The chemical state of iron in reduced PdFe Al<sub>2</sub>O<sub>3</sub> catalysts. *J. Catal.* **1974**, *35*, 232–246. [[CrossRef](#)]
170. Garten, R.L. Direct evidence for bimetallic clusters. *J. Catal.* **1976**, *43*, 18–33. [[CrossRef](#)]
171. Kadinov, G.; Bonev, C.; Todorova, S.; Palazov, A.; Lietz, G.; Völter, J. Infrared study of carbon monoxide adsorption and hydrogenation over PdFe catalysts. *J. Mol. Catal.* **1993**, *83*, 157–166. [[CrossRef](#)]
172. Pârvulescu, V.I.; Filoti, G.; Pârvulescu, V.; Grecu, N.; Angelescu, E.; Nicolescu, I.V. Styrene hydrogenation on supported Pd, Fe and PdFe/ $\gamma$ -Al<sub>2</sub>O<sub>3</sub> catalysts. *J. Mol. Catal.* **1994**, *89*, 267–282. [[CrossRef](#)]
173. Golubina, E.V.; Lokteva, E.S.; Lunin, V.V.; Telegina, N.S.; Stakheev, A.Y.; Tundo, P. The role of Fe addition on the activity of Pd containing catalysts in multiphase hydrodechlorination. *Appl. Catal. A Gen.* **2006**, *302*, 32–41. [[CrossRef](#)]
174. Tarasevich, M.R.; Zhutaeva, G.V.; Bogdanovskaya, V.A.; Radina, M.V.; Ehrenburg, M.R.; Chalykh, A.E. Oxygen kinetics and mechanism at electrocatalysts on the base of palladium iron system. *Electrochim. Acta* **2007**, *52*, 5108–5118. [[CrossRef](#)]
175. Jin, Y.; Ma, C.; Shi, M.; Chu, Y.; Xu, Y.; Huang, T.; Huang, Q.; Miao, Y. Highly active carbon nanotube supported bimetallic palladium iron electrocatalysts for formic acid electro oxidation. *Int. J. Electrochem. Sci.* **2012**, *7*, 3399–3408.
176. Yeh, Y.C.; Chen, H.M.; Liu, R.S.; Asakura, K.; Lo, M.Y.; Peng, Y.M.; Chan, T.S.; Lee, J.F. PdFe nanoparticles investigated by X-ray absorption spectroscopy as electrocatalysts for oxygen reduction. *Chem. Mater.* **2009**, *21*, 4030–4036. [[CrossRef](#)]
177. Yang, J.; Zhou, W.; Cheng, C.H.; Lee, J.Y.; Liu, Z. Pt decorated PdFe nanoparticles as methanol tolerant oxygen reduction electrocatalyst. *ACS Appl. Mater. Interfaces* **2010**, *2*, 119–126. [[CrossRef](#)] [[PubMed](#)]
178. Wang, W.; Wang, R.; Ji, S.; Feng, H.; Wang, H.; Lei, Z. Pt overgrowth on carbon supported PdFe seeds in the preparation of core shell electrocatalysts for the oxygen reduction reaction. *J. Power Sources* **2010**, *195*, 3498–3503. [[CrossRef](#)]
179. Yin, S.; Cai, M.; Wang, C.; Shen, P.K. Tungsten carbide promoted PdFe as alcohol tolerant electrocatalysts for oxygen reduction reactions. *Energy Environ. Sci.* **2011**, *4*, 558–563. [[CrossRef](#)]
180. Alexeyeva, N.; Sarapuu, A.; Tammeveski, K.; Vidallglesiás, F.J.; SollaGullón, J.; Feliu, J.M. Electro reduction of oxygen on Vulcan carbon supported Pd nanoparticles and PdM nanoalloys in acid and alkaline solutions. *Electrochim. Acta* **2011**, *56*, 6702–6708. [[CrossRef](#)]
181. Wang, H.; Ji, S.; Wang, W.; Linkov, V.; Pasupathi, S.; Wang, R. Pt decorated PdFe/C: Extremely high electrocatalytic activity for methanol oxidation International. *J. Electrochem. Sci.* **2012**, *7*, 3390–3398.
182. Pires, F.I.; Villullas, H.M. Pd-based catalysts: Influence of the second metal on their stability and oxygen reduction activity. *Int. J. Hydrogen Energy* **2012**, *37*, 17052–17059. [[CrossRef](#)]
183. Rivera Gavidia, L.M.; García, G.; Anaya, D.; Querejeta, A.; Alcaide, F.; Pastor, E. Carbon supported Pt-free catalysts with high specificity and activity toward the oxygen reduction reaction in acidic medium. *Appl. Catal. B Environ.* **2016**, *184*, 12–19. [[CrossRef](#)]
184. Polshettiwar, V.; Nadagouda, M.N.; Varma, R.S. Microwave assisted chemistry: A rapid and sustainable route to synthesis of organics and nanomaterials. *Aust. J. Chem.* **2009**, *62*, 16–26. [[CrossRef](#)]

185. Holade, Y.; Da Silva, R.G.; Servat, K.; Napporn, T.W.; Canaff, C.; De Andrade, A.R.; Kokoh, K.B. Facile synthesis of highly active and durable PdM/C ( $M = \text{Fe, Mn}$ ) nanocatalysts for the oxygen reduction reaction in an alkaline medium. *J. Mater. Chem. A* **2016**, *4*, 8337–8349. [[CrossRef](#)]
186. Homeyer, S.T.; Sheu, L.L.; Zhang, Z.; Sachtler, W.M.H.; Balse, V.R.; Dumesic, J.A. Chemical interaction of palladium particles with iron cations in NaY. *Appl. Catal.* **1990**, *64*, 225–241. [[CrossRef](#)]
187. Choudary, B.M.; Lázár, K.; Bogyay, I.; Gucci, L. Promotion effect of Fe on the selectivity of Pd zeoliteX in methanol synthesis. *J. Chem. Soc. Faraday Trans.* **1990**, *86*, 419–424. [[CrossRef](#)]
188. Wen, B.; Jia, J.; Sachtler, W.M.H. Chemical anchoring of palladium by Fe Oxo ions in zeolite ZSM-5. *J. Phys. Chem. B* **2002**, *106*, 7520–7523. [[CrossRef](#)]
189. Hinokuma, S.; Katsuhara, Y.; Ando, E.; Ikeue, K.; Machida, M. PdFe/CeO<sub>2</sub> bimetal catalysts prepared by dual arc-plasma deposition. *Catal. Today* **2013**, *201*, 92–97. [[CrossRef](#)]
190. Mizuno, N.; Misono, M. Heterogeneous catalysis. *Chem. Rev.* **1998**, *98*, 199–218. [[CrossRef](#)]
191. Campanati, M.; Fornasari, G.; Vaccari, A. Fundamentals in the preparation of heterogeneous catalysts. *Catal. Today* **2003**, *77*, 299–314. [[CrossRef](#)]
192. LePage, J.F.; Ertl, G.; Knözinger, H.; Weitkamp, J. *Handbook of Heterogeneous Catalysis*; Wiley/VCH: New York, NY, USA; Weinheim, Germany, 1997; Volume 1, p. 49.
193. Musolino, M.G.; Busacca, C.; Mauriello, F.; Pietropaolo, R. Aliphatic carbonyl reduction promoted by palladium catalysts under mild conditions. *Appl. Catal. A Gen.* **2010**, *379*, 77–86. [[CrossRef](#)]
194. Zhang, Y.; Cao, H.; Zhang, J.; Xia, B. Synthesis of LiNi<sub>0.6</sub>Co<sub>0.2</sub>Mn<sub>0.2</sub>O<sub>2</sub> cathode material by a carbonate co-precipitation method and its electrochemical characterization. *Solid State Ion.* **2006**, *177*, 3303–3307. [[CrossRef](#)]
195. Cho, T.H.; Shiosaki, Y.; Noguchi, H. Preparation and characterization of layered LiMn<sub>1/3</sub>Ni<sub>1/3</sub>Co<sub>1/3</sub>O<sub>2</sub> as a cathode material by an oxalate co-precipitation method. *J. Power Sources* **2006**, *159*, 1322–1327. [[CrossRef](#)]
196. Lee, S.H.; Georgii, I.N. Transfer hydrogenation of ketones, nitriles, and esters catalyzed by a half-sandwich complex of Ruthenium. *ChemCatChem* **2015**, *7*, 107–113. [[CrossRef](#)]
197. Yang, L.; Chen, X.; Zhou, Z.; Zhang, R.; Li, L.; Cheng, Z.; Fang, X. Magnetic Fe<sub>3</sub>O<sub>4</sub>@SiO<sub>2</sub>/Pd and Fe<sub>3</sub>O<sub>4</sub>@SiO<sub>2</sub>/Pd-M ( $M = \text{Ag, Cu and Zn}$ ) catalysts for selective hydrogenation of phenylacetylene. *ChemistrySelect* **2016**, *1*, 5599–5606. [[CrossRef](#)]
198. Deng, H.; Li, X.; Peng, Q.; Wang, X.; Chen, J.; Li, Y. Monodisperse magnetic single-crystal ferrite microspheres. *Angew. Chem. Int. Ed.* **2005**, *44*, 2782–2785. [[CrossRef](#)] [[PubMed](#)]
199. Bunaciu, A.A.; Udriștioiu, E.G.; Aboul-Enein, H.Y. X-ray diffraction: Instrumentation and applications. *Crit. Rev. Anal. Chem.* **2015**, *45*, 289–299. [[CrossRef](#)] [[PubMed](#)]
200. Thibault, P.; Elser, V. X-ray diffraction microscopy. *Annu. Rev. Condens. Matter Phys.* **2010**, *1*, 237–255. [[CrossRef](#)]
201. Datye, A.K.; Smith, D.J. The study of heterogeneous catalysts by high-resolution electron microscopy. *Catal. Rev.* **1992**, *34*, 129–178. [[CrossRef](#)]
202. Yang, J.C.; Small, M.W.; Griesshaber, R.V.; Nuzzo, R.G. Recent developments and applications of electron microscopy to heterogeneous catalysis. *Chem. Soc. Rev.* **2012**, *41*, 8179–8194. [[CrossRef](#)] [[PubMed](#)]
203. Thomas, J.M.; Midgley, P.A. High-resolution transmission electron microscopy: The ultimate nanoanalytical technique. *Chem. Commun.* **2004**, 1253–1267. [[CrossRef](#)] [[PubMed](#)]
204. Datye, A.K. Electron microscopy of catalysts: Recent achievements and future prospects. *J. Catal.* **2003**, *216*, 144–154. [[CrossRef](#)]
205. International Center for Diffraction Data. *Powder Diffraction Database*; International Center for Diffraction Data: Pennsylvania, PA, USA, 1997.
206. Feio, L.S.F.; Hori, C.E.; Mattos, L.V.; Zanchet, D.; Noronha, F.B.; Bueno, J.M.C. Partial oxidation and autothermal reforming of methane on Pd/CeO<sub>2</sub>-Al<sub>2</sub>O<sub>3</sub> catalysts. *Appl. Catal. A Gen.* **2008**, *348*, 183–192. [[CrossRef](#)]
207. Neri, G.; Rizzo, G.; De Luca, L.; Donato, A.; Musolino, M.G.; Pietropaolo, R. Supported Pd catalysts for the hydrogenation of campholenic aldehyde: Influence of support and preparation method. *Appl. Catal. A Gen.* **2009**, *356*, 113–120. [[CrossRef](#)]
208. Braunstein, P.; Devenish, R.; Gallezot, P.; Heaton, B.T.; Hurnphreys, C.J.; Kervennal, J.; Muliey, S.; Ries, M. Silica-supported Fe-Pd bimetallic particles: Formation from mixed-metal clusters and catalytic activity. *Angew. Chem. Int. Ed.* **1988**, *27*, 927–929. [[CrossRef](#)]

209. Hensley, A.J.R.; Hong, Y.; Zhang, R.; Zhang, H.; Sun, J.; Wang, Y.; McEwen, J.-S. Enhanced Fe<sub>2</sub>O<sub>3</sub> reducibility via surface modification with Pd: Characterizing the synergy within Pd/Fe catalysts for hydrodeoxygenation reactions. *ACS Catal.* **2014**, *4*, 3381–3392. [[CrossRef](#)]
210. Li, Z.Q.; Lu, C.J.; Xia, Z.P.; Zhou, Y.; Luo, Z. X-ray diffraction patterns of graphite and turbostratic carbon. *Carbon* **2007**, *45*, 1686–1695. [[CrossRef](#)]
211. Liao, M.; Hu, Q.; Zheng, J.; Li, Y.; Zhou, H.; Zhong, C.-J.; Chen, B.H. Pd decorated Fe/C nanocatalyst for formic acid electro oxidation. *Electrochim. Acta* **2013**, *111*, 504–509. [[CrossRef](#)]
212. Wang, W.; Zheng, D.; Du, C.; Zou, Z.; Zhang, X.; Xia, B.; Yang, H.; Akins, D.L. Carbon-supported Pd-Co bimetallic nanoparticles as electrocatalysts for the oxygen reduction reaction. *J. Power Sources* **2007**, *167*, 243–249. [[CrossRef](#)]
213. Hurst, N.W.; Gentry, S.J.; Jones, A.; McNicol, B.D. Temperature programmed reduction. *Catal. Rev.* **1982**, *24*, 233–309. [[CrossRef](#)]
214. Chou, C.-W.; Chu, S.-J.; Chiang, H.-J.; Huang, C.-Y.; Lee, C.-J.; Sheen, S.-R.; Perng, T.P.; Yeh, C.-T. Temperature-programmed reduction study on calcination of nano-Palladium. *J. Phys. Chem. B* **2001**, *105*, 9113–9117. [[CrossRef](#)]
215. Gil, S.; Garcia-Vargas, J.M.; Liotta, L.F.; Pantaleo, G.; Ousmane, M.; Retailleau, L.; Giroir-Fendler, A. Catalytic oxidation of propene over Pd catalysts supported on CeO<sub>2</sub>, TiO<sub>2</sub>, Al<sub>2</sub>O<sub>3</sub> and M/Al<sub>2</sub>O<sub>3</sub> Oxides (M = Ce, Ti, Fe, Mn). *Catalysts* **2015**, *5*, 671–689. [[CrossRef](#)]
216. Tiernan, M.J.; Barnes, P.A.; Parkes, G.M.B. Reduction of iron oxide catalysts: The investigation of kinetic parameters using rate perturbation and linear heating thermoanalytical techniques. *J. Phys. Chem. B* **2001**, *105*, 220–228. [[CrossRef](#)]
217. Lin, H.Y.; Chen, Y.W.; Li, C. The mechanism of reduction of iron oxide by hydrogen. *Thermochim. Acta* **2003**, *400*, 61–67. [[CrossRef](#)]
218. Turner, N.H.; Schreifels, J.A. Surface Analysis: X-ray photoelectron spectroscopy and auger electron spectroscopy. *Anal. Chem.* **1996**, *68*, 309–332. [[CrossRef](#)]
219. Van der Heide, P. *X-ray Photoelectron Spectroscopy: An Introduction to Principles and Practices*; John Wiley & Sons, Inc.: Hoboken, NJ, USA, 2012.
220. Winograd, N.; Gaarenstroom, S.W. *X-ray Photoelectron Spectroscopy, Physical Methods in Modern Chemical Analysis*; Academic Press, Inc./Elsevier Inc.: New York, NY, USA, 1980; Volume 2, pp. 115–169.
221. Sharpe, L.R.; Heineman, W.R.; Elder, R.C. EXAFS spectro-electrochemistry. *Chem. Rev.* **1990**, *90*, 705–722. [[CrossRef](#)]
222. Gaur, A.; Shrivastava, B.D.; Nigam, H.L. X-ray Absorption fine structure (XAFS) spectroscopy—A review. *Proc. Indian Natl. Sci. Acad.* **2013**, *79*, 921–966.
223. Asakura, K. Recent developments in the in situ XAFS and related work for the characterization of catalysts in Japan. *Catal. Surv. Asia* **2003**, *7*, 177–182. [[CrossRef](#)]
224. Schlaf, M. Selective deoxygenation of sugar polyols to  $\alpha,\omega$ -diols and other oxygen content reduced materials—A new challenge to homogeneous ionic hydrogenation and hydrogenolysis catalysis. *Dalton Trans.* **2006**, *39*, 4645–4653. [[CrossRef](#)] [[PubMed](#)]
225. Martin, A.; Armbruster, U.; Gandarias, I.; Arias, P.L. Glycerol hydrogenolysis into propanediols using in situ generated hydrogen—A critical review. *Eur. J. Lipid Sci. Technol.* **2013**, *115*, 9–27. [[CrossRef](#)]
226. Gandarias, I.; Arias, P.L.; Requies, J.; El Doukkali, M.; Güemez, M.B. Liquid-phase glycerol hydrogenolysis to 1,2-propanediol under nitrogen pressure using 2-propanol as hydrogen source. *J. Catal.* **2011**, *282*, 237–247. [[CrossRef](#)]
227. Yue, H.; Zhao, Y.; Ma, X.; Gong, J. Ethylene glycol: Properties, synthesis, and applications. *Chem. Soc. Rev.* **2012**, *41*, 4218–4244. [[CrossRef](#)] [[PubMed](#)]
228. Zheng, M.; Pang, J.; Wang, A.; Zhang, T. One-pot catalytic conversion of cellulose to ethylene glycol and other chemicals: From fundamental discovery to potential commercialization. *Chin. J. Catal.* **2014**, *35*, 602–613. [[CrossRef](#)]
229. Wang, A.; Zhang, T. One-pot conversion of cellulose to ethylene glycol with multifunctional Tungsten-based catalysts. *Acc. Chem. Res.* **2013**, *46*, 1377–1386. [[CrossRef](#)] [[PubMed](#)]
230. Luo, Y.R. *Comprehensive Handbook of Chemical Bond Energies*; CRC Press: Boca Raton, FL, USA, 2007.

231. Saliccioli, M.; Yu, W.; Barteau, M.A.; Chen, J.G.; Vlachos, D.G. Differentiation of O–H and C–H bond scission mechanisms of ethylene glycol on Pt and Ni/Pt using theory and isotopic labeling experiments. *J. Am. Chem. Soc.* **2011**, *133*, 7996–8004. [[CrossRef](#)] [[PubMed](#)]
232. Bennett, R.A.; Pang, C.L.; Perkins, N.; Smith, R.D.; Morrall, P.; Kvon, R.I.; Bowker, M. Surface structures in the SMSI state; Pd on (1 × 2) reconstructed TiO<sub>2</sub>(110). *J. Phys. Chem. B* **2002**, *106*, 4688–4696. [[CrossRef](#)]
233. Dulub, O.; Hebenstreit, W.; Diebold, U. Imaging cluster surfaces with atomic resolution: The strong metal-support interaction state of Pt supported on TiO<sub>2</sub> (110). *Phys. Rev. Lett.* **2000**, *84*, 3646–3649. [[CrossRef](#)] [[PubMed](#)]
234. Alhanash, A.; Kozhevnikova, E.F.; Kozhevnikov, I.V. Hydrogenolysis of glycerol to propanediol over Ru-polyoxometalate bifunctional catalyst. *Catal. Lett.* **2007**, *120*, 307–311. [[CrossRef](#)]
235. Balaraju, M.; Rekha, V.; Sai Prasad, P.S.; Prasad, R.B.N.; Lingaiah, N. Selective hydrogenolysis of glycerol to 1,2 propanediol over Cu–ZnO catalysts. *Catal. Lett.* **2008**, *126*, 119–124. [[CrossRef](#)]
236. Hattori, H. Heterogeneous basic catalysis. *Chem. Rev.* **1995**, *95*, 537–558. [[CrossRef](#)]
237. Hattori, H. Solid base catalysts: Generation of basic sites and application to organic synthesis. *Appl. Catal. A Gen.* **2001**, *222*, 247–259. [[CrossRef](#)]
238. Bernas, J.H.; Taskinen, A.; Wärnå, J.; Murzin, D.Y. Describing the inverse dependence of hydrogen pressure by multi-site adsorption of the reactant: Hydrogenolysis of hydroxymatairesinol on a Pd/C catalyst. *J. Mol. Catal. A Chem.* **2009**, *306*, 33–39. [[CrossRef](#)]
239. Frusteri, F.; Italiano, G.; Espro, C.; Arena, F. CH<sub>4</sub> Decomposition on Ni and Co thin layer catalysts to produce H<sub>2</sub> for fuel cell. *Catal. Today* **2011**, *171*, 60–66. [[CrossRef](#)]
240. Vannice, M.A.; Garten, R.L. Supported Palladium catalysts for methanation. *Ind. Eng. Chem. Prod. Res. Dev.* **1979**, *18*, 186–191. [[CrossRef](#)]
241. Deutsch, K.L.; Lahr, D.G.; Shanks, B.H. Probing the ruthenium-catalyzed higher polyol hydrogenolysis reaction through the use of stereoisomers. *Green Chem.* **2012**, *14*, 1635–1642. [[CrossRef](#)]
242. Shanks, B.H. Conversion of biorenewable feedstocks: New challenges in heterogeneous catalysis. *Ind. Eng. Chem. Res.* **2010**, *49*, 10212–10217. [[CrossRef](#)]
243. Sohounloue, D.K.; Montassier, C.; Barbier, J. Catalytic hydrogenolysis of sorbitol. *React. Kinet. Catal. Lett.* **1983**, *22*, 391–397. [[CrossRef](#)]
244. Li, N.; Huber, G.W. Aqueous-phase hydrodeoxygenation of sorbitol with Pt/SiO<sub>2</sub>–Al<sub>2</sub>O<sub>3</sub>: Identification of reaction intermediates. *J. Catal.* **2010**, *270*, 48–59. [[CrossRef](#)]
245. Rinaldi, R. (Ed.) *Catalytic Hydrogenation for Biomass Valorization*; RSC Energy and Environment Series No. 13; The Royal Society of Chemistry: London, UK, 2015; pp. 1–310.
246. Moreno, B.M.; Li, N.; Lee, J.; Huber, G.W.; Klein, M.T. Modeling aqueous-phase hydrodeoxygenation of sorbitol over Pt/SiO<sub>2</sub>–Al<sub>2</sub>O<sub>3</sub>. *RSC Adv.* **2013**, *3*, 23769–23784. [[CrossRef](#)]
247. Huber, G.W.; Cortright, R.D.; Dumesic, J.A. Renewable alkanes by aqueous-phase reforming of biomass-derived oxygenates. *Angew. Chem. Int. Ed.* **2004**, *43*, 1549–1551. [[CrossRef](#)] [[PubMed](#)]
248. Kim, Y.T.; Dumesic, J.A.; Huber, G.W. Aqueous-phase hydrodeoxygenation of sorbitol: A comparative study of Pt/Zr phosphate and Pt-ReOx/C. *J. Catal.* **2013**, *304*, 72–85. [[CrossRef](#)]
249. Li, B.D.; Wang, J.; Yuan, Y.Z.; Ariga, H.; Takakusagi, S.; Asakura, K. Carbon nanotube-supported RuFe bimetallic nanoparticles as efficient and robust catalysts for aqueous-phase selective hydrogenolysis of glycerol to glycols. *ACS Catal.* **2011**, *1*, 1521–1528. [[CrossRef](#)]
250. Frontera, P.; Macario, A.; Aloise, A.; Antonucci, P.; Giordano, G.; Nagy, J.B. Effect of support surface on methane dry-reforming catalyst preparation. *Catal. Today* **2013**, *218*, 18–29. [[CrossRef](#)]
251. Lo Faro, M.; Frontera, P.; Antonucci, P.; Aricò, A.S. Ni-Cu based catalysts prepared by two different methods and their catalytic activity toward the ATR of methane. *Chem. Eng. Res. Des.* **2015**, *93*, 269–277. [[CrossRef](#)]
252. Frontera, P.; Aloise, A.; MacArio, A.; Crea, F.; Antonucci, P.; Giordano, G.; Nagy, J.B. Zeolite-supported Ni catalyst for methane reforming with carbon dioxide. *Res. Chem. Intermed.* **2015**, *37*, 267–279. [[CrossRef](#)]
253. Yamaguchi, A.; Hiyoshi, N.; Sato, O.; Shirai, M. Sorbitol dehydration in high temperature liquid water. *Green Chem.* **2011**, *13*, 873–881. [[CrossRef](#)]
254. Karinen, R.; Vilonen, K.; Niemelä, M. Biorefining: Heterogeneously catalyzed reactions of carbohydrates for the production of furfural and hydroxymethylfurfural. *ChemSusChem* **2011**, *4*, 1002–1016. [[CrossRef](#)] [[PubMed](#)]

255. Binder, J.B.; Blank, J.J.; Cefali, A.V.; Raines, R.T. Synthesis of furfural from xylose and xylan. *ChemSusChem* **2010**, *3*, 1268–1272. [[CrossRef](#)] [[PubMed](#)]
256. Aellig, C.; Hermans, I. Continuous D-fructose dehydration to 5-Hydroxymethylfurfural under mild conditions. *ChemSusChem* **2012**, *5*, 1737–1742. [[CrossRef](#)] [[PubMed](#)]
257. Zheng, R.Y.; Zhu, Y.X.; Chen, J.G.G. Promoting low-temperature hydrogenation of C=O bonds of acetone and acetaldehyde by using Co–Pt bimetallic catalysts. *ChemCatChem* **2011**, *3*, 578–581. [[CrossRef](#)]
258. Zheng, R.Y.; Humbert, M.P.; Zhu, Y.X.; Chen, J.G. Low-temperature hydrogenation of the C=O bond of propanal over Ni–Pt bimetallic catalysts: From model surfaces to supported catalysts. *Catal. Sci. Technol.* **2011**, *1*, 638–643. [[CrossRef](#)]
259. Wang, H.; Male, J.; Wang, Y. Recent advances in hydrotreating of pyrolysis bio-oil and its oxygen-containing model compound. *ACS Catal.* **2013**, *3*, 1047–1070. [[CrossRef](#)]
260. Huber, G.W.; Iborra, S.; Corma, A. Synthesis of transportation fuels from biomass: Chemistry, catalysts, and engineering. *Chem. Rev.* **2006**, *106*, 4044–4098. [[CrossRef](#)] [[PubMed](#)]
261. Mohan, D.; Pittman, C.U.; Steele, P.H. Pyrolysis of wood/biomass for bio-oil: A critical review. *Energy Fuels* **2006**, *20*, 848–889. [[CrossRef](#)]
262. Shafaghat, H.; Rezaeia, P.S.; Daud, W.M.A.W. Effective parameters on selective catalytic hydrodeoxygenation of phenolic compounds of pyrolysis bio-oil to high-value hydrocarbons. *RSC Adv.* **2015**, *5*, 103999–104042. [[CrossRef](#)]
263. Saidi, M.; Samimi, F.; Karimipourfard, D.; Nimmanwudipong, T.; Gates, B.C.; Rahimpour, M.R. Upgrading of lignin-derived bio-oils by catalytic hydrodeoxygenation. *Energy Environ. Sci.* **2014**, *7*, 103–129. [[CrossRef](#)]
264. Song, W.; Liu, Y.; Baráth, E.; Zhao, C.; Lercher, J.A. Synergistic effects of Ni and acid sites for hydrogenation and C–O bond cleavage of substituted phenol. *Green Chem.* **2015**, *17*, 1204–1218. [[CrossRef](#)]
265. Grilc, M.; Likozar, B.; Levec, J. Hydrodeoxygenation and hydrocracking of solvolysed lignocellulosic biomass by oxide, reduced and sulphide form of NiMo, Ni, Mo and Pd catalysts. *Appl. Catal. B Environ.* **2014**, *150–151*, 275–287. [[CrossRef](#)]
266. Hensley, A.J. R.; Wang, Y.; McEwen, J.S. Phenol deoxygenation mechanisms on Fe(110) and Pd(111). *ACS Catal.* **2015**, *5*, 523–536. [[CrossRef](#)]
267. Bolognini, M.; Cavani, F.; Scagliarini, D.; Flego, C.; Perego, C.; Saba, M. Heterogeneous basic catalysts as alternatives to homogeneous catalysts: Reactivity of Mg/Al mixed oxides in the alkylation of m-cresol with methanol. *Catal. Today* **2002**, *75*, 103–111. [[CrossRef](#)]
268. Gu, G.H.; Mullen, C.A.; Boateng, A.A.; Vlachos, D.G. Mechanism of dehydration of phenols on noble metals via first-principles microkinetic modeling. *ACS Catal.* **2016**, *6*, 3047–3055. [[CrossRef](#)]
269. Shafaghat, H.; Rezaei, P.S.; Daud, W.M.A.W. Catalytic hydrogenation of phenol, cresol and guaiacol over physically mixed catalysts of Pd/C and zeolite solid acids. *RSC Adv.* **2015**, *5*, 33990–33998. [[CrossRef](#)]
270. Cozzula, D.; Vinci, A.; Mauriello, F.; Pietropaolo, R.; Müller, T.E. Directing the cleavage of ester C–O bonds by controlling the hydrogen availability on the surface of coprecipitated Pd/Fe<sub>3</sub>O<sub>4</sub>. *ChemCatChem* **2016**, *8*, 1515–1522. [[CrossRef](#)]

